Pergamon

Geochimica et Cosmochimica Acta, Vol. 59, No. 3, pp. 593–612, 1995

0016-7037/95 $9.50 + .00

0016-7037(94)00384-X

Classification and origin of IAB and IIICD iron meteorites

BYEON-GAK CHOI,[1,2] XINWEI OUYANG,[1] and JOHN T. WASSON[1,2,3]

[1] Institute of Geophysics and Planetary Physics, University of California, Los Angeles, CA 90024, USA
[2] Department of Earth and Space Sciences, University of California, Los Angeles, CA 90024, USA
[3] Department of Chemistry and Biochemistry, University of California, Los Angeles, CA 90024, USA

(*Received May* 24, 1994; *accepted in revised form October* 26, 1994)

Abstract—We have analyzed, by duplicate neutron-activation analysis, 125 members of iron meteorite groups IAB and IIICD. These data show no hiatus between the groups, and we recommend that the two sets be treated as a single group until data are obtained that require their separation. In cases where there is no ambiguity, we will use IAB to designate the combined group.

Our data allow properties of group IAB to be more tightly constrained than heretofore. We examined the properties of ungrouped irons occupying the same region of Ga-Ni and Ge-Ni space as IAB and found that our more precise data did not add any to the group. Based primarily on Co-Ni, Au-Ni, and to a lesser extent, Cu-Ni and As-Ni trends we find that three irons (Hassi-Jekna, Magnesia and Qarat al Hanash) previously assigned to IIICD are better designated ungrouped, primarily because their Au contents diverge from those of IAB; six irons (EET 84300, Mertzon, Misteca, Persimmon Creek, Yongning, and Zacatecas (1792)) have also been removed from IAB on the basis of the new data.

Fractional crystallization models of magmas saturated in troilite yield trends for several elements quite similar to those observed in IAB and, with moderate modification of the distribution coefficients, these can also account for the IIICD trend. However, this model requires metal segregation and convective stirring at very low temperatures, and predicts a much lower abundance of low-Ni irons than observed. It also fails to account for the ubiquitous presence of trapped melt and chondritic (or subchondritic) silicates in IAB irons.

The weight of the evidence supports an impact-melt model in which individual IAB irons are interpreted as melt pools produced by impacts into a chondritic megaregolith. The lower the melt temperature of the melt, the larger the fraction of Ga, Ge, and Ir that remained sequestered in unmelted solids. The increasing range in Ga, Ge, and Ir with increasing Ni content can be explained by mixing between different primary melt pools having compositions along the lower (IIICD) envelope of IAB-IIICD. And we suggest that some high-Ni melt pools having low cotectic temperatures experienced crystal settling on a scale of cm to m; specifically, this process may be responsible for producing the most Ni-rich members of the group. We infer that the IAB precursor materials had properties (high porosity, fine grain size) that made them susceptible to impact melting. A high FeS would also favor melt generation. The oxygen isotope composition of IAB silicates is 0.45‰ below the terrestrial-fractionation line in a region occupied by CR chondrites and other carbonaceous-chondrite-related meteorites. This suggests that the chondritic precursor was a metal- and FeS-rich carbonaceous chondrite.

Cl-normalized element/Ni ratios in low-Ni (65–68 mg/g) IAB are ≥1.5 for Co, Ga, Ge, and Au. Although the high Ga and Ge abundance ratio could indicate fractional crystallization of elements having high solid/melt distribution coefficients, this explanation cannot account for the Co and Au enrichments. We interpret the high Ga, Ge, and Au ratios in terms of a nebular condensation-accretion model; we suggest that these elements condensed into a late-formed, fine nebular component having an enhanced abundance in the chondritic materials parental to group IAB. Because it is more refractory than Fe and Co, the Ni content of this fine metal was appreciably lower than that of the early formed coarse metal.

INTRODUCTION

The iron meteorite groups are divided into two classes, the magmatic and the nonmagmatic irons. Both models involve melting, but the nonmagmatic melts seem to have had small dimensions (< a few tens of m) and never to have been hot enough to have had a low viscosity. The magmatic groups (epitomized by groups IIAB and IIIAB) show large ranges in elemental concentrations (especially for refractories such as Ir) and strong interelement correlations. Silicates are rare and, in most cases consist of SiO_2. The large ranges in elemental concentration seems to require that these groups formed by fractional crystallization of a well-mixed magma, and all other evidence is consistent with this interpretation.

The three nonmagmatic groups (IAB, IIE, and IIICD) show less strong interelement correlations and lower ranges for most elements Ni (Ga and Ge are the exceptions). Silicates are common and relatively primitive; in IAB, many silicates clasts are cm-size and have chondritic or subchondritic (i.e., nearly chondritic) compositions. They contain planetary-type noble gases and have formation ages comparable to those found in chondrites. In IIE, the composition of most silicates is consistent with formation as melt extracted from chondritic matter (i.e., chondritic matter less olivine) or as chondritic matter minus metal and FeS; noble gases concentrations are much lower than in IAB but planetary-type interelement ratios are generally recognizable (e.g., in Watson—Olsen et al., 1994).

Fractional crystallization requires efficient mixing of the residual magma. Primarily because large chondritic inclusions are found throughout the compositional range of IAB (from Campo del Cielo with 65 mg/g Ni, 400 mg/g Ge, and 4 μg/g Ir to San Cristobal with 250 mg/g Ni, 25 mg/g Ge, and 0.5 μg/g Ir), Wasson (1970) concluded that IAB irons had not been melted during the period since the silicates and metal were mixed.

Wasson (1972) summarized the evidence for separating the iron meteorite groups into magmatic and nonmagmatic classes (he used the terms igneous and nonigneous) including the small size of parental γ-iron crystals in nonmagmatic IAB compared to magmatic IIIAB, despite very similar cooling rates at temperatures in the range 750–950 K when the Widmanstätten pattern was forming.

It has proven quite difficult to find a satisfactory model for the origin of IAB irons. Wasson (1970) suggested that metal and silicates were mechanically separated in the solar nebula, and that the large metallic regions formed by solid-state growth during metamorphism. Wasson et al. (1980) proposed that the metal was molten, but only very briefly as a result of impact heating events. Each IAB iron was inferred to comprise a separate melt pool, and the variations in elemental composition attributed to differing degrees of melting of precursor chondritic silicates.

Kelly and Larimer (1977) concluded that IAB did not form by fractional crystallization. They proposed low-degree fractional melting of a chondritic precursor in which successive melts never recombine but undergo "premature refreezing" as separate pods.

Kracher (1982, 1985) suggested that IAB irons could have formed by the fractional crystallization of a "core or a small number of very large melt pools," providing the magma had a very high S content. The role of the high S content was to modify the elemental distribution between melt and solids such that observed trends are consistent with fractional crystallization. During much of the crystallization history both metal and troilite were cocrystallizing.

In order to better assess the origin of IAB-IIICD irons we have analyzed essentially all members of this set by instrumental neutron activation analysis (INAA).

ANALYTICAL TECHNIQUES AND RESULTS

Our INAA procedure was described by Wasson et al. (1989). Samples 3-mm thick and having masses in the range 450–650 mg are analyzed in duplicate and additional analyses added in those cases where one or more elements fail to agree within about four sample standard deviations (s). We included pieces of the Filomena specimen of the North Chile IIAB iron and of NBS steel 809B as standards in each INAA run. The standard for Re was an aqueous solution pipetted onto hydrophilic polyethylene 3 mm thick.

In most of the irradiations, we also included a sample of Canyon Diablo specimen UCLA 965 and in some irradiations, Odessa specimen UCLA 420B. The Canyon Diablo dataset published by Wasson and Ouyang (1990) can be used to assess the precision of our technique. They reported data on Canyon Diablo specimen LC965 analyzed in twenty-one different INAA runs over a period of seven years. The observed relative sample standard deviation are ≤4% for Co, Ni, Cu, Ga, and Ir, 6–9% for Au, 12–13% for Sb, W, Re, and Pt, and 24% for Cr. These should be generally applicable to our IAB analyses; they are listed at the bottom of Table 1. The high scatter in Cr probably indicates that an appreciable fraction is present in chromite that is not uniformly sampled by our technique.

Mean INAA concentrations of twelve elements and RNAA concentrations for Ge in IAB and IIICD irons are listed in Table 1. As will be discussed in detail, the border between IAB and IIICD is arbitrary, and it appears probable that these irons should be assigned to the same group. For that reason, irons are listed in alphabetical order in Table 1, independent of group assignment. Current group assignments are shown, but persons using this table should bear in mind their arbitrary nature. Also included in Table 1 are the number of replicate analyses included in the mean. In most cases where three or more replicates were determined, the additional analysis was needed to resolve a discrepancy in the first two analyses. The final column lists the elements that failed to yield concordant data because of discrepancies. To help the reader find IAB-IIICD irons having a particular composition, we prepared lists sorted in terms of Ni, Ga, and Ir; these are in Appendix I.

A number of ungrouped irons have compositions that place them close to the IAB-IIICD fields on Ga-Ni and Ge-Ni log-log diagrams. Mean compositional data for these ungrouped irons are listed in Table 2. We describe how these irons were selected in the following section.

CLASSIFICATION

Resolution of IAB and IIICD from Similar Ungrouped Irons, Based on Metal Composition Data

The term group is used by meteorite researchers to designate sets of meteorites similar enough in their properties to imply origin in a single parent body (for chondrites) or a limited portion of a parent body (for igneously formed meteorites). We use three additional related terms: the modifier ungrouped is applied to those meteorites that do not belong to a set with five or more members. In some cases, it is convenient to designate these small sets of closely related meteorites grouplets. The term anomalous member of a group we apply only to those meteorites that share most properties with the members of a group, but differ significantly (e.g., by 2–3 s) in two or more key properties. For example, the properties of the Mundrabilla iron are consistent with membership in IIICD with the exception of the low Ir in the metal, about a factor 2 outside the main field, and its very high concentration of troilite, which is about 6× greater than typical of IAB-IIICD (Kracher and Wasson, 1982).

Among the iron meteorites as a whole the elements Ga and Ge remain the best taxonomic parameters because of their narrow ranges within groups but wide ranges among the entire set of irons. Although these elements show wide ranges in IAB-IIICD, in combination with Ni they still offer an excellent screen to separate IAB-IIICD and other related irons from hoi polloi. Figures 1a and b show Ga-Ni and Ge-Ni log-log diagrams for all iron meteorites studied by this research group.

In general, IAB and IIICD irons have higher Ga and Ge values than those of other iron meteorites with similar Ni contents. To examine whether any irons previously classified as ungrouped might actually belong to IAB-IIICD, the ungrouped irons having values higher than the straight lines in Fig. 1 were selected for further examination. Among the ungrouped meteorites having Ga or Ge values lower than the lines, only Kendall County and Zacatecas (1792) were included in this set. We also excluded irons having Ge/Ga outside the IAB-IIICD range. For IAB-IIICD, we calculated the regression lines $\log Ge = 1.51 \cdot \log Ga - 0.376$; if a Ge value differed from that predicted by this line by a factor > 2, the iron was excluded from the list, and not examined further. The sole exception is Ni-rich Oktibbeha County, which we

Table 1. Mean concentrations of siderophile elements in 126 IAB and IIICD irons. Letters used as labels in diagrams are shown bold.

meteorite	group +	++	Cr µg/g	Co mg/g	Ni mg/g	Cu µg/g	Ga µg/g	Ge* µg/g	As µg/g	Sb ng/g	W ng/g	Re ng/g	Ir µg/g	Pt µg/g	Au µg/g	**
Alexander County	IAB	2	29	4.56	64.7	142	100.4	518	11.2	260	1730	330	3.73	11.0	1.44	
Allan Hills A77283	IAB	2	25	4.81	74.7	146	80.4	320	15.4	440	1080	260	2.04		1.72	
Annaheim	IAB -An	4	20	4.69	78.8	500	79.6	302	13.5	380	1160	360	3.60		1.58	
Anoka	IIICD	2	21	5.60	118.8	193	17.4	16	20.6	480	110		0.16	<1.2	1.58	
Bahjoi	IAB	2	21	4.83	78.7	159	66.0	265	17.1	530	960	300	2.50	5.8	1.75	
Balfour Downs	IAB	2	22	4.87	83.8	161	59.4	194	16.6	400	1270	240	2.15		1.70	
Ballinger (AMNH)	IIICD	2	13	4.61	64.8	133	83.9	350	13.9	320	1050	240	2.21	7.2	1.55	
Ballinger (UCLA)	IAB	4	26	4.61	67.9	148	87.8	358	12.1	340	1260	320	3.20	6.4	1.52	
Bischtübe	IAB	3	23	5.02	72.7	135	68.0	238	16.8	360	700	210	2.31	5.7	1.65	
Black Mountain	IAB	2	23	4.66	64.6	128	96.3	460	12.0	270	1430	340	2.92		1.52	Ni
Bogou	IAB	2	24	4.67	73.0	163	79.4	301	14.2	300	1090	200	1.72		1.65	
Bohumilitz	IAB	2	21	4.76	72.2	134	77.6	264	15.4	360	880	220	2.04		1.60	
Bolivia	IAB	4	22	4.64	68.6	152	96.4	377	11.3	320	1350	210	2.15	8.7	1.50	
Burgavli	IIICD	2	28	4.45	65.9	168	97.0	519	11.0		1900	170	1.18		1.44	
Burkett	IAB	2	20	4.65	69.5	170	88.9	368	13.5	510	1510	250	2.48		1.65	
Caddo County	IAB	2	185	4.91	91.7	360	68.1	246	14.8	400	1110	320	2.55	7.5	1.61	
California	IAB	2	17	4.95	79.7	171	68.4	253	16.4	330	830	270	2.58		1.71	
Campo del Cielo	IAB	4	40	4.37	71.3	136	91.0	392	10.8	280	1320	320	3.19	6.7	1.48	
Canyon Diablo	IAB	64	25	4.66	70.1	152	81.8	327	13.1	290	1110	250	2.32	6.2	1.56	
Carlton	IIICD	3	18	5.69	132.8	263	11.9	8.6	23.5	570	260	<60	0.08		1.75	
Casey County	IIICD	3	22	4.68	70.0	163	80.6	317	13.7	540	1240	160	1.33		1.62	
Colfax	IAB	4	14	5.27	107.6	333	53.6	153	17.9	540	540	160	1.73		1.67	
Comanche (iron)	IAB	2	19	4.99	81.9	176	76.2	262	17.0	430	890	230	2.69	6.1	1.72	
Cookeville	IAB	3	27	4.31	69.7	153	88.1	384	13.3	290	1170	250	2.48	9.0	1.72	
Coolac	IAB	3	33	4.46	69.7	156	91.0	423	11.6	280	1300	290	2.73	8.1	1.53	
Copiapo	IAB	3	77	4.82	74.0	163	72.3	252	14.5	330	950	290	2.93		1.68	
Cosby's Creek	IAB	2	23	4.46	64.9	155	92.9	431	11.5	270	1820	320	2.72		1.45	
Cranbourne	IIICD	2	26	4.60	69.4	139	84.9	306	13.1	350	1180	180	1.70		1.55	
Dayton"	IIICD	2	19	5.57	170.3	525	5.1	3.6	25.6		90	<60	0.03		1.96	Co,Au
Deelfontein	IAB	5	24	4.59	72.3	168	80.3	306	15.5	340	1530	210	1.68	4.5	1.63	Ni,Ga
Deport	IAB	2	19	4.73	80.4	177	64.6	255	17.2	420	1120	260	2.37		1.69	
Duel Hill (1873)	IAB	2	13	4.85	67.1	163	104.0	426	11.4	280	1440	400	4.52		1.51	
Dungannon	IAB	2	27	4.72	71.0	153	78.7	330	13.6	350	950	240	2.66	6.0	1.65	
Edmonton (KY)	IIICD	2	21	5.48	129.0	404	24.4	35	21.3	470	290	<150	0.50		1.71	
Egvekinot	IIICD	2	11	5.62	143.0	359	12.6	9.9	24.4	720	190		0.10		1.97	Au
Elephant Moraine 83333	IAB	2	19	4.88	80.6	184	74.8	226	15.7	450	800	280	2.88	6.8	1.75	
Ellicott	IAB	2	18	4.91	75.4	175	61.5	252	13.6	190	1500	310	3.46		1.41	
Fairfield	IIICD	2	19	4.67	66.1	141	78.4	329	12.9	360	1000	160	1.79	5.8	1.55	
Föllinge	IIICD	2	12	5.96	177.3	371	3.9	3.2	26.4	840	<70	<20	0.11	<1.1	1.70	
Four Corners	IAB	2	31	5.09	90.0	243	49.0	179	16.2	480	600	240	2.43	5.3	1.65	
Freda	IIICD	2	11	6.30	232.9	672	2.1	2.2	30.4	1280	<90	<40	0.02	<1.8	1.90	
Georgetown	IIICD -An	1	2790	5.12	90.1	347	58.3	251	18.4	370	720	<45	0.25	3.6	1.52	
Gladstone (iron)	IAB	4	21	4.75	68.2	150	88.9	418	12.2	300	1390	300	2.79	6.9	1.51	
Goose Lake	IAB	3	31	4.86	82.2	169	68.6	305	16.5	390	1000	220	2.13	6.0	1.64	
Harlowton	IAB -An	2	<25	4.93	88.7	433	59.8	222	15.9	510	660	240	2.49		1.60	
Hasparos	IAB	2	27	4.66	65.7	155	101.7	486	12.4	<870	1730	510	5.62		1.55	
Hatfield	IAB	2	32	5.00	79.8	141	61.9	238	15.9	400	830	240	2.56	4.9	1.57	
Hope	IIICD	3	23	4.58	70.1	152	90.6	388	11.7	370	1380	50	0.75		1.54	
Idaho	IAB	2	19	4.66	72.2	157	83.9	321	13.5	310	1060	260	2.49		1.61	
Itapuranga	IAB	3	29	4.88	64.5	134	94.3	478	11.4	310	1650	260	2.63	9.7	1.58	
Jaralito	IIICD	3	32	4.68	67.3	147	89.4	376	11.7	340	1290	170	1.49		1.59	
Jenkins	IAB	4	25	4.55	69.2	151	87.6	353	13.1	340	1300	250	2.16		1.58	
Jenny's Creek	IAB	3	23	4.71	68.3	141	81.7	320	13.6	350	1140	280	2.41	5.7	1.63	
Karee Kloof	IAB	2	35	4.71	83.8	231	80.4	355	15.0	470	1270	100	1.29		1.58	
Lamesa	IIICD	3	12	5.61	131.3	326	13.2	11	24.0	590	<100	<20	0.04	<0.6	1.82	
Landes	IAB -An	4	445	4.49	65.8	320	89.9	425	10.6	340	1480	320	4.26		1.42	
Leeds	IAB	2	20	4.82	82.5	176	68.9	241	15.7	410	820	220	2.45		1.71	
Lewis Cliff 86540	IIICD	2	12	5.99	182.9	479	4.3	2.8	28.8	790	<60	<20	0.04	2.0	1.81	
Lexington County	IAB	2	20	4.59	68.3	155	81.6	316	13.8	300	1120	290	2.86		1.56	
Linwood	IAB	4	11	4.61	69.1	136	91.1	374	12.1	300	1240	290	2.78		1.59	
Magura	IAB	3	26	4.62	64.8	142	98.2	483	10.5	180	1800	360	3.60		1.53	
Maltahöhe	IIICD	2	15	5.26	113.6	163	24.0	38	19.2	480	200	<50	0.18	1.9	1.47	Ni,Pt,Au
Masua	IAB	3	22	4.96	78.2	172	69.2	250	16.6	420	770	260	2.04	5.8	1.70	
Mayerthorpe	IAB	3	21	4.75	70.6	139	79.1	283	15.2	320	1390	240	2.18	3.1	1.63	
Mazapil	IAB -An	2	9	5.17	88.7	220	62.0	221	18.5	540	750	470	5.95		1.83	
Mesa Verde Park	IAB	2	19	4.96	120.7	355	63.1	142	18.9	450	600	420	2.17	5.0	1.87	

tentatively leave in group IAB even though it has a Ge/Ga ratio a factor of 3 higher than the line. As noted by Kracher and Willis (1981), Oktibbeha County lies on or near IAB trends on all log *X*-log Ni diagrams. Ungrouped irons that were excluded on the basis of this screen were Y791076, EET87506, and ALH80104. The remaining ungrouped irons are listed in Table 2 and are closely related to IAB-IIICD irons in terms of Ga-Ni and Ge-Ni relationships.

We then used four additional log *X* vs. log Ni diagrams to distinguish the core members of IAB-IIICD from ungrouped irons (Fig. 2), and to reevaluate the assignment of irons previously included in these groups. The envelopes sketched on these diagrams show the core compositional ranges of IAB-IIICD irons. Irons that plot well outside the core are identified by abbreviations based on the meteorite name; the letters used are shown in bold in Tables 1 and 2.

Table 1 (continued).

meteorite	group +	++	Cr µg/g	Co mg/g	Ni mg/g	Cu µg/g	Ga µg/g	Ge* µg/g	As µg/g	Sb ng/g	W ng/g	Re ng/g	Ir µg/g	Pt µg/g	Au µg/g	**
Morasko	IIICD	4	25	4.54	68.5	158	103.6	496	10.9	170	1740	90	1.10		1.52	
Morrill	IAB	2	13	4.81	82.5	279	64.0	296	15.7	440	930	200	1.60	6.6	1.66	
Mount Ayliff	IAB	1	23	4.92	73.4	125	75.1	250	15.5		790	280	2.03	5.4	1.63	
Mundrabilla	IIICD -An	2	241	4.95	74.7	125	58.0	196	15.4	390	550	90	0.91		1.66	
Mungindi	IIICD	2	15	5.50	119.3	248	18.8	22	22.4	480	<70	80	0.55	1.5	1.67	
Nagy-Vazsony	IAB	2	17	4.99	80.5	188	72.0	263	18.4	420	800	280	2.48	6.1	1.79	
Nantan	IIICD	9	31	4.63	70.3	150	82.1	293	12.8	360	1130	180	1.71	5.1	1.59	
Neptune Mountains	IAB	2	20	4.73	72.0	149	76.6	269	14.4	320	910	200	2.19		1.63	
New Leipzig	IAB	3	16	4.68	66.0	150	90.9	445	11.3	230	1530	280	2.83		1.46	
Niagara	IAB	2	14	5.12	78.8	172	72.0	266	17.0	400	800	270	2.71	5.1	1.78	
Ocotillo	IAB	2	22	4.65	70.9	116	72.3	288	13.7	330	810	260	2.61	5.5	1.66	
Odessa	IAB	30	33	4.71	71.9	130	75.6	283	14.4	310	1270	240	2.40	6.2	1.65	
Ogallala	IAB	1	29	4.76	79.7	155	67.4	266	15.7		1020	310	2.48	6.6	1.63	
Oktibbeha County	IAB	2	21	5.03	608	6220	3.6	9.0	31.0	38550	750		0.03		1.66	Au
Oscuro Mountains	IAB	3	22	4.51	69.7	179	80.2	359	12.2	270	1180	270	2.96		1.59	
Osseo	IAB	2	26	4.58	65.1	159	91.1	450	10.7	310	1470	530	5.85		1.52	
Ozren	IAB	1	27	4.80	69.3	134	79.6	331	14.2		1100	190	2.61	4.0	1.57	
Pan de Azucar	IAB	3	24	4.70	69.2	169	83.0	318	12.2	300	1130	300	2.81	3.6	1.52	
Paracutu	IAB	2	44	4.85	75.6	140	74.7	320	16.5	380	1370	330	2.77		1.72	
Pecora Escarpment 91003	IAB	2	29	4.62	70.8	148	82.6	313	13.0	430	1110	270	3.61	5.9	1.50	
Pine River	IAB	3	9	4.78	83.2	194	67.9	234	14.9	380	680	280	3.05	5.0	1.54	Ni,Ga
Pitts	IAB	2	14	5.06	127.0	376	35.1	94	20.2	940	350	110	1.22	3.1	1.72	
Pittsburg	IIICD	2	16	4.70	65.8	130	89.3	339	14.6	300	1080	240	2.13	6.4	1.64	
Pooposo	IAB	3	44	4.57	71.1	199	80.6	325	11.9	320	1040	230	2.68		1.53	
Pugatory Peak A77006	IAB	2	29	4.68	72.6	142	81.3	284	14.3	420	1000	260	2.11		1.65	
Reckling Peak A80226	IAB	2	23	4.88	82.9	173	67.8	255	17.1		900	220	2.06		1.74	
Rifle	IIICD	4	24	4.68	70.1	134	76.8	282	14.4	350	890	210	1.92	4.9	1.59	
Rosario	IAB	3	20	4.75	70.6	153	88.5	401	12.0	280	1240	190	1.83		1.58	
San Cristobal	IAB	1	17	6.22	249.7	934	11.1	25	28.9	2170	<90	<30	0.33	<2.9	2.05	
Sardis	IAB	2	16	4.61	67.1	138	97.4	420	12.1	280	1300	270	2.01		1.52	
Sarepta	IAB	3	34	4.70	66.9	150	98.3	457	11.5	330	1470	420	4.01		1.49	
Seeläsgen	IIICD	3	25	4.52	66.5	159	102.9	493	10.7	250	1850	110	1.15		1.53	
Seligman	IAB	2	28	4.59	66.9	162	94.1	423	12.0	340	1280	330	3.30	7.2	1.49	
Seymour	IIICD	3	30	4.80	68.9	159	86.7	382	12.9	230	1250	190	1.67		1.60	
Shrewsbury	IAB	2	16	4.88	85.6	217	63.0	204	17.3	430	610	260	2.77		1.75	
Silver Crown	IAB	2	28	4.61	72.0	143	83.8	321	12.8	310	1010	290	2.81		1.66	
Smithville	IAB	2	22	4.67	70.2	162	89.0	363	14.1	340	1930	230	1.90	5.7	1.47	Ga,W
Soledade	IAB	2	21	4.57	67.8	147	98.6	440	11.1	320	1430	390	3.90	9.7	1.47	
Southern Arizona	IAB	2	26	4.91	82.0	176	69.9	242	17.1	370	1080	240	2.46	5.8	1.71	
Surprise Springs	IAB	1	39	4.75	81.3	191	66.8	265	14.3	400	720	240	2.24	4.6	1.69	
Tazewell	IIICD	3	13	5.83	172.1	399	4.8	3.8	26.7	680	120	<20	0.09	<2.7	1.81	
Thiel Mountains 91725	IAB	2	209	4.70	79.3	174	73.6	243	12.7	490	1020	250	3.67	6.2	1.53	
Thompson Brook	IIICD	1	17	5.03	76.5	136	59.7	173	17.5	430	620	110	1.04	4.3	1.66	
Toluca	IAB	7	18	4.89	78.6	163	69.0	254	16.8	400	810	270	2.39	6.1	1.67	
Udei Station	IAB	3	32	4.81	97.1	257	69.3	204	15.2	640	790	130	0.68		1.62	
Vaalbult	IAB	2	26	4.53	68.3	145	83.7	323	14.8		1240	280	2.13		1.60	
Waldron Ridge	IAB	2	38	4.65	78.0	274	76.8	282	12.0	300	1020	250	2.21	6.4	1.50	
Waterville	IIICD -An	2	677	4.68	76.5	245	64.5	196	15.2	360	510	<60	0.35		1.54	Cu,W,Re
Waverley	IAB -An	2	22	4.65	88.6	326	77.5	365	14.9	450	1140	110	0.97	4.7	1.53	
Wichita County	IIICD	2	28	4.66	67.9	149	83.8	341	12.4	370	1200	210	1.90		1.57	
Wolsey	IAB	2	43	4.52	66.2	137	92.8	459	10.5	260	1560	480	4.86	10.3	1.46	
Woodbine	IAB	2	73	5.42	97.0	165	35.2	114	17.8	520	620	210	1.97		1.64	
Wooster	IAB	2	18	4.82	78.1	174	66.2	258	15.2		850	250	2.58		1.65	
Yamato 791694	IAB	1	8	5.67	342	1973	12.2	37	34.2	3980			0.24		1.86	
Yardea	IAB	3	18	4.56	73.3	182	87.2	361	11.3	310	1340	380	4.32		1.54	
Yardymly	IIICD	2	27	4.44	67.4	157	87.7	387	11.9	320	1520	210	1.55		1.65	
Yenberrie	IAB	4	29	4.72	71.0	159	83.0	315	12.6	370	1040	320	3.50	5.7	1.57	
Youndegin	IAB	7	24	4.70	68.0	143	85.0	334	13.0	310	1070	220	2.15	5.4	1.55	
Zagora	IAB	2	77	4.80	97.0	257	66.3	226	15.1	350	910	280	2.74	6.6	1.60	
Zenda	IAB	2	13	5.02	87.9	223	51.4	214	16.7	400	750	290	2.47		1.79	
Mean of low Ni IAB-IIICD^			41	4.62	66.2	159	93.0	425	11.8	300	1450	300	3.02	7.9	1.52	
S.D in Canyon Diablo^^			24	3.2	2.4	4.1	4.0	5.9	5.6	13	13	12	3.1	13	6.9	

\# unpublished data of E.Scott, Ni data from RNAA
\+ An = anomalous member of the group
++ number of INAA replicates
* RNAA data if available
** elements that show discrepancies between replicates
^ Mean of IAB-IIICD irons having Ni values ≤68 mg/g
^^ relative sample standard deviation of 21 Canyon Diablo analyses (in %)

Their distance from the core was calculated from the ratio X_{obs}/X_{reg} where X_{obs} is the observed concentration and X_{reg} is the concentration calculated by inserting the observed Ni concentration into the regression relationship fitted to the core set.

Most remaining ungrouped irons were excluded based on these diagrams, especially the Co-Ni and Au-Ni diagrams. For example, note particularly the deviant positions on the Au-Ni diagram (Fig. 2d) of the irons Hassi-Jekna, Magnesia, and Qarat al Hanash that were previously assigned to IIICD (Wasson et al., 1980; Malvin et al., 1984). Because Au is an element we determine with very high precision, the positions of these three irons about 4s away from the IAB-IIICD trend convinced us to reclassify them as ungrouped. They also plot outside the IAB-IIICD core on the As-Ni diagram (Fig. 2c), but their separation is less pronounced.

Table 2. Mean conentrations of siderophile elements in 22 ungrouped irons closely related to IAB-IIICD

meteorite	+	Cr µg/g	Co mg/g	Ni mg/g	Cu µg/g	Ga µg/g	Ge* µg/g	As µg/g	Sb ng/g	W ng/g	Re ng/g	Ir µg/g	Pt µg/g	Au µg/g	**
Algarrabo	2	25	4.41	82.9	281	66.8	321	15.0	360	1200	980	10.1	8.6	1.47	
Algoma	3	<30	5.51	105.8	264	20.4	38	25.9	<240	230	<100	0.35		2.41	
Elephant Moraine 84300	2	84	5.10	102.2	192	41.3	92	13.9	400	330	180	1.82	2.6	1.29	
Garden Head	2	8	6.27	174.6	426	10.9	17	23.3	340	170	<30	0.10		2.49	Ir
Gay Gulch	2	13	6.93	152.4	235	6.2	11	21.2	340	400	<20	0.11		2.68	
Hassi-Jekna	2	17	5.53	107.2	177	24.2	70	26.6	350	210	<20	0.23	1.5	2.40	
Kendall County	3	200	3.96	55.0	443	73.1	355	10.8	730	1040	280	2.00	1.5	1.37	
Kofa	2	7	7.23	186.7	452	4.7	8.6	28.4	650	340	<200	0.10		2.97	
Linville	2	<70	5.92	165.7	278	7.6	16	29.1		<120	<120	0.07		2.90	
Livingston TN	2	32	4.15	72.1	296	56.9	250	13.4	400	830	90	0.77	4.8	1.43	Sb
Magnesia	3	26	5.36	106.8	247	14.4	22	23.6	250	210	<40	0.14		2.73	
Mertzon	5	118	4.02	94.5	673	67.1	293	13.1	540	1010	220	2.28		1.55	
Misteca	3	21	5.44	84.0	168	68.5	233	18.9	530	740	290	2.66	7.1	2.15	Ir,Au
Muzaffarpur	2	44	6.06	139.9	213	15.3	29	32.2	430	380	80	0.55		3.36	
Persimmon Creek	2	32	5.37	137.8	374	32.1	78	15.5	610	220	110	0.84		1.51	
Qarat al Hanash	2	34	5.56	127.5	212	16.7	29.7	26.7	390	270	100	0.85		2.78	
Quesa	2	<100	6.34	119.5	285	33.1		23.0		2700	<60	0.13		2.48	W
Santa Catharina	3	10	6.17	359	1436	5.2	8.8	38.3	2770	200	<40	0.03		3.64	
Twin City	2	<15	6.17	306	1143	4.5	7.4	37.7	2340	<120	<150	0.02		3.68	Co
Yongning	2	34	4.07	65.0	151	96.5	490	10.6	340	2040	370	3.69		1.48	
Zacatecas(1792)	2	155	4.80	59.9	123	80.8	307	6.8	90	1910	130	2.14	11.7	0.74	

\+ number of INAA replicates between replicates
* RNAA data if available
** elements that show discrepancies between replicates

The Cu-Ni and As-Ni diagrams do not offer the same level of discrimination as the Co-Ni and Au-Ni diagrams, but do show that a few irons having more or less normal contents of Co and Au should be assigned to the ungrouped or anomalous member categories. Yongning, Mertzon, and Livingston TN have Co contents distinctly lower than IAB-IIICD, and Quesa, Gay Gulch, and Kofa have high Co contents. Livingston TN and Mertzon also have anomalously high Cu and are classified ungrouped. Algarrabo is designated ungrouped because of its slightly low Co and its extremely high Ir (about four times higher than those of IAB with similar Ni contents). Landes, Annaheim, and Harlowton have Cu contents distinctly outside the IAB core and are designated anomalous IAB members because of this one anomalous property.

The speculation of Wasson et al. (1980) that As contents are significantly higher in IIICD than in IAB is not confirmed

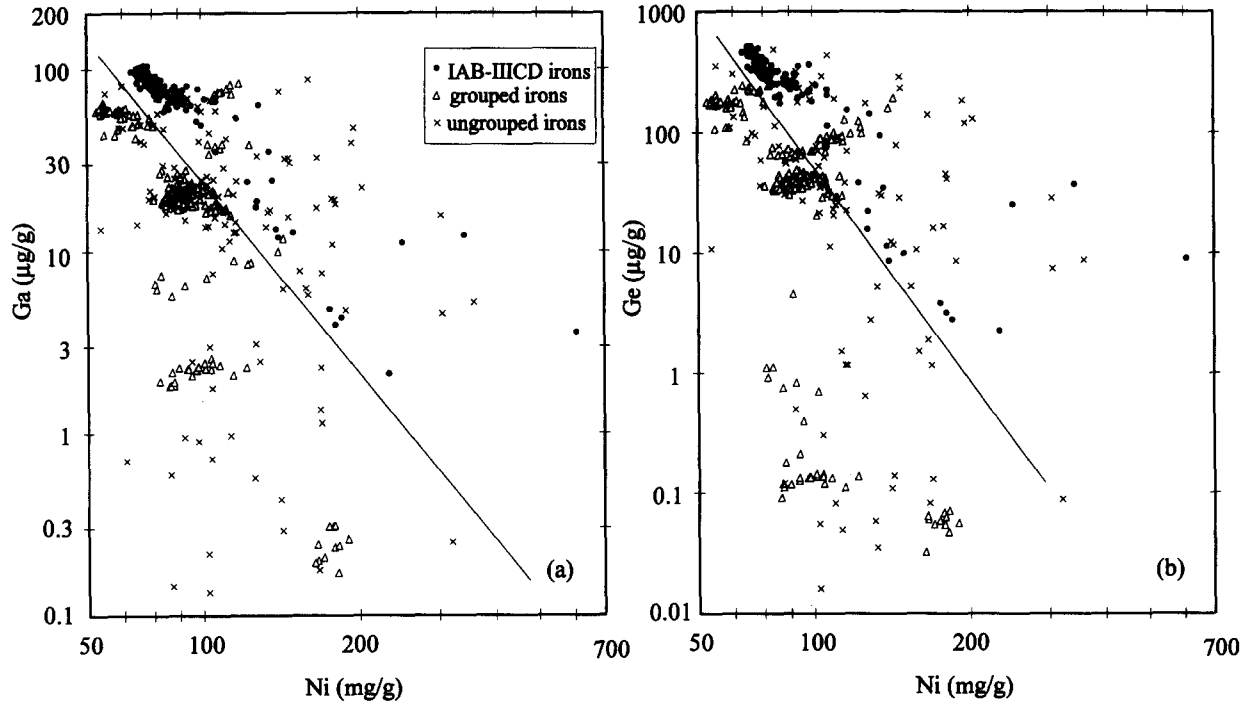

FIG. 1. Log-log diagrams of (a) Ga vs. Ni and (b) Ge vs. Ni, showing all iron meteorites analyzed by this research group. Diagonal lines delineate the IAB-IIICD fields as defined by these and other properties (see text). We reexamined the properties of all ungrouped irons falling within these regions on both diagrams.

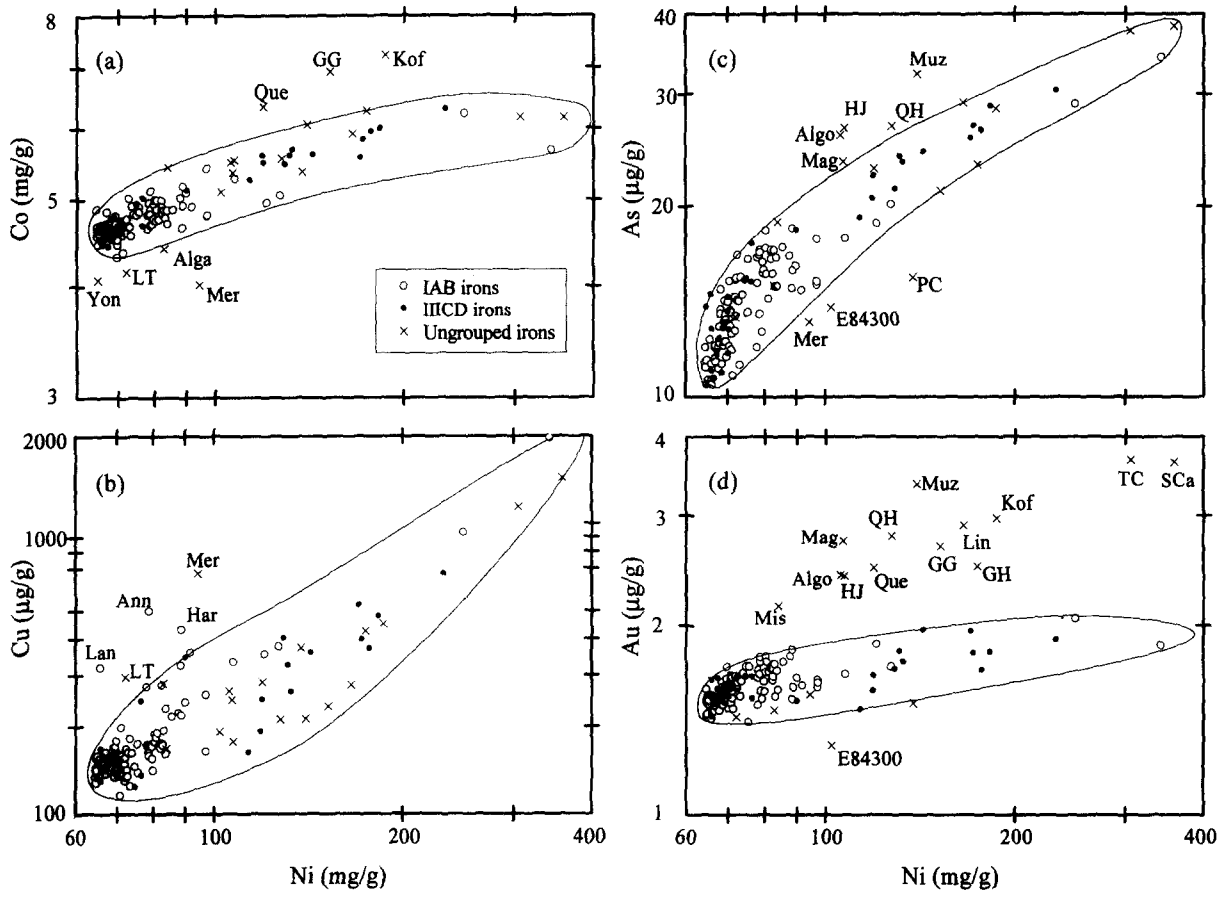

FIG. 2. Log-log diagrams of (a) Co, (b) Cu, (c) As, and (d) Au vs. Ni for irons belonging to groups IAB and IIICD and a set of ungrouped irons chosen as described in connection with Fig. 1. The fields within which nearly all IAB and IIICD irons plot are indicated. Irons plotting $>3s$ from the centers on these fields on two or more diagrams are designated ungrouped. Irons plotting $>3s$ but $<4s$ from the centers of these fields on a single diagram are designated anomalous members of group IAB-IIICD.

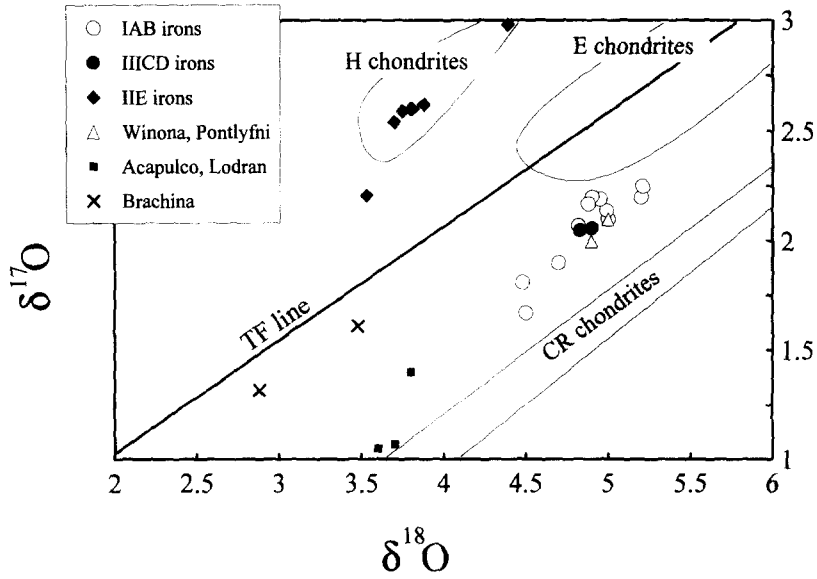

FIG. 3. Oxygen isotopes in the silicate inclusions of IAB-IIICD irons form a tight cluster at $\delta^{18}O = 5‰$, $\Delta^{17}O = 0.45‰$; the Winona and Pontlyfni chondrites are in the same cluster. The CR chondrite field passes just below the cluster. Data from Clayton and Mayeda (1978), Clayton et al. (1983), Clayton et al. (1984), Clayton et al. (1991), Mayeda and Clayton (1980), and Weisberg et al. (1993).

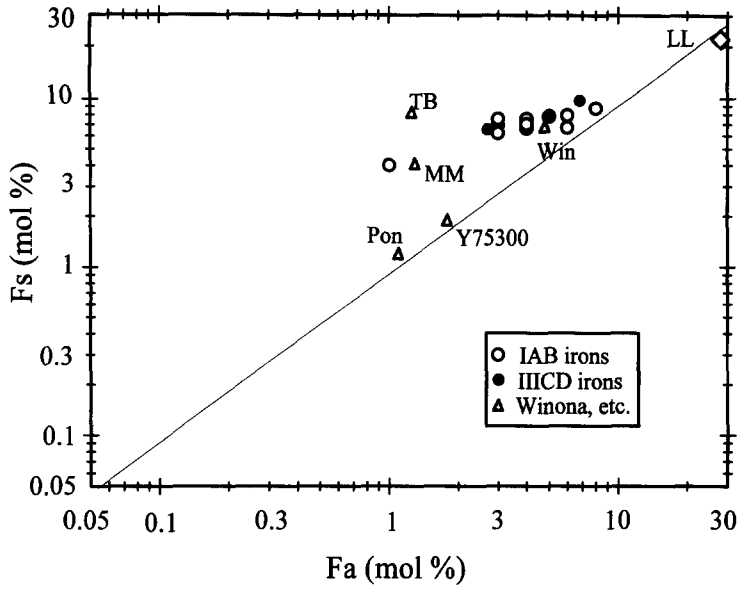

FIG. 4. In contrast to the relationship produced by equilibrium, in IAB-IIICD silicates the Fe/(Fe + Mg) ratio in low-Ca pyroxene is higher than that in the coexisting olivine. This indicates that the assemblage has experienced a late reduction. Diffusion rates are higher in olivine than in pyroxene, resulting in more efficient reduction of the olivine. Data from Bunch et al. (1970), Bild (1977), McCoy et al. (1993), King et al. (1981), Kimura et al. (1992), and Graham et al. (1977).

by this much more extensive and precise dataset. Among low-Ni irons there is no tendency of the two sets to be resolved on Fig. 2c.

If one or two properties deviated from the core field by a relatively small amount ($\approx 2-3s$ from the center of the field) we designated it an anomalous member of IAB or IIICD. Irons with IAB-IIICD compositions but having distinct mineral assemblages, for example, anomalously large troilite contents, were also designated anomalous members. When the deviation in one property was particularly large ($>4s$), even if only one element is anomalous, we classified the iron ungrouped. The resulting classifications appear in Tables 1 and 2.

Properties of IAB-IIICD Silicates and Those of Related Chondrites

Many IAB-IIICD irons contain angular blocks of silicates. The mineralogy of these materials is basically chondritic; by mass they consist of roughly 70% mafic silicates, 10% sodic plagioclase, 10% metal, and 10% sulfide; the largest inclusions reach sizes of at least 8 cm (Fig. 1 in Wlotzka and Jarosewich, 1977). The silicates are relatively reduced; with few exceptions, pyroxene compositions are in the range 6–9 mol% Fs. Many other IAB-IIICD irons contain much smaller amounts of silicates, generally in troilite-graphite inclusions. Although we do not have the observations to prove it, we suspect that all IAB-IIICD irons contain silicates.

In Fig. 3, we show the published bulk oxygen isotope analyses for IAB silicates and several related chondrites. Also shown are data for other meteorites whose bulk oxygen isotope compositions are in the same portion of the three-isotope diagram. Most authors who have examined the petrography of the closely related chondrites Pontlyfni, Winona, and Mount Morris WI have concluded that these chondrites are close relatives of the IAB-IIICD silicates. We suggest that it is reasonable to assign them all to the same group, i.e., to IAB.

The oxygen isotope compositions of the IAB silicates fall distinctly below the terrestrial-fractionation line at $\Delta^{17}O$ ($=\delta^{17}O - 0.52 \cdot \delta^{18}O$) $\approx -0.45‰$ (Clayton, 1993). This is one indication that the IAB meteorites are more closely related to carbonaceous chondrites than to ordinary chondrites. As will be discussed in more detail later, their high contents of volatile elements including C is another indication.

The olivine of IAB meteorites is more reduced than the low-Ca pyroxene. Figure 4 shows a plot of pyroxene composition versus olivine composition. The olivine Fa contents are uniformly lower than the values expected from equilibrium with the low-Ca pyroxene. Kallemeyn and Wasson (1985) noted that, because olivine equilibrates more rapidly with imposed redox conditions than pyroxene, this sort of distribution implies a late reduction of the assemblage from an original composition that was at least as FeO-rich as the most ferroan pyroxene.

This leads to the interesting problem of assessing the original FeO/(FeO + MgO) in the IAB silicates. We assume that they were all as ferroan as the most ferroan pyroxenes known, those in Udei Station having Fs contents of 8.3 mol%. Since the olivine in Udei Station is reduced relative to the pyroxene, it is possible that the original pyroxene composition was still more ferroan.

As discussed in more detail below, the IAB meteorites contain large amounts of reduced C as graphite and carbides. It seems probable that these were the reducing agents that lowered the FeO contents of the silicates. Graphite is only a strong reducing agent if the CO partial pressure is low. This may not have been a constraint for small silicate inclusions in large amounts of metal, but could have played a significant role in

limiting the amount of reduction in regions having high silicate/metal ratios and high overburden pressures.

The IAB-IIICD silicates contain large amounts of primordial noble gases; reported $^{36}Ar_p$ and $^{132}Xe_p$ contents are in the range $(2-4)\cdot10^{-8}$ cm^3 g^{-1} and $(2-8)\cdot10^{-10}$ cm^3 g^{-1}, respectively (Niemeyer, 1979a,b). These are roughly comparable to the amounts in type-4 ordinary chondrites (Marti, 1967). The maximum metamorphism temperatures of type-4 ordinary chondrites are estimated to be about 870–970 K (Dodd, 1981).

Difficulty in Resolving IAB and IIICD

The three key trends that were used by Wasson et al. (1980) to separate IAB from IIICD were Ga-Ni, Ge-Ni, and Ir-Ni. As described above, we now use other taxonomic parameters (especially Co-Ni and Au-Ni diagrams) to eliminate some meteorites from the combined set. In Fig. 5, we show these pruned datasets on Ga-Ni, Ge-Ni, and Ir-Ni diagrams. We followed the general practice of Wasson et al. (1980) to separate low-Ni irons into IAB and IIICD portions, and arbitrarily used the combination of Ga, Ge, and Ir to set the border between IAB and IIICD. We assigned Ir (which shows more variation at low Ni concentrations), twice as much weight as Ga and Ge in the geometric mean and defined as IIICD those meteorites falling below the line: $\log((Ga\cdot Ge)^{0.5}\cdot Ir)^{0.5} = -2.428\cdot\log Ni + 5.707$. As shown in Fig. 6, this line leads to a clean separation of irons having Ni contents >72 mg/g, but at lower Ni contents there is no hiatus and the decision on where to place the line is quite arbitrary. Our choice minimizes the amount of reassignment relative to the group designations by Wasson et al. (1980).

We now examine whether there are indications in the compositions of the metal or the silicates that this division is meaningful. McCoy et al. (1993) studied the silicates in the new IIICD iron Maltahöhe and also in IIICD Dayton, and plotted these pyroxene and plagioclase compositions together with literature data for other IAB-IIICD irons vs. the mean Ni content of the metal. Figure 7 is an updated version of this diagram. To the three IIICD irons that McCoy et al. (1993) included we added IIICD-an Mundrabilla. This has the effect of strengthening the positive IIICD trend between pyroxene Fs and Ni and generating a negative trend between plagioclase An and Ni.

In our opinion, the low plagioclase An in Carlton and Dayton mainly reflects the partitioning of the Ca between plagioclase and the phosphates that are appreciably more abundant. As a result, plagioclase compositions no longer preserve information about possible initial IAB-IIICD differences in silicate composition. McCoy et al. suggest that this explanation cannot account for the low An of Maltahöhe, but we question whether its phosphate/plagioclase ratio is well enough known to rule this explanation out.

Because mafic silicates are also rare in Carlton and Dayton, we suspect that they have reequilibrated during metamorphism. Most of the studied IAB silicates consisted of blocks with dimensions greater than 1 cm, large enough to have potentially preserved approximate starting compositions. In contrast, silicates in Carlton and Dayton are tiny and rare, and were probably appreciably altered by late metamorphic reequilibration.

MODELING THE ELEMENTAL TRENDS IN IAB-IIICD METAL

Historical Overview

It has long been recognized that siderophile-Ni trends in the metal of IAB irons differed from those in other iron-meteorite groups (Wasson, 1970). When it became clear that the ubiquitous silicates were essentially chondritic, contained planetary-type rare gases, and had very old formation ages and well resolved I-Xe formation intervals, many researchers abandoned the standard iron-meteorite formation model, fractional crystallization of a core (Wasson, 1972; Scott and Bild, 1974; Kelly and Larimer, 1977).

The solution proposed by Kelly and Larimer (1977) was that small subsets of IAB irons formed in magma pools produced by (sequential) partial melting in a planetary interior. This model falters because the FeS should enter fully into the first of these partial melts, whereas FeS is ubiquitous among IAB-IIICD irons. The model also requires a very high mean Ni content in the precursor metal in order to explain the high-Ni contents of the earliest melts, those responsible for the high-Ni irons. A high mean Ni content is inconsistent with the observation that 90% of IAB-IIICD irons have Ni contents <90 mg/g, and that these irons have much larger recovered masses than the high-Ni irons.

In the first version of the impact model we endorse in this paper, Wasson et al. (1980) proposed that each IAB iron was formed by incomplete melting, and that each of these melt pools was produced by impact heating in a chondritic megaregolith. The observed trends were attributed to differing degrees of equilibration of the impact melt with the unmelted residue. Low-Ni melts reached high temperatures and were able to extract a large fraction of the siderophiles from the unmelted solids. At the high-Ni extreme, only metal adjacent to troilite was melted, and the melts chilled before diffusional exchange with the unmelted solids could occur; the siderophiles that became incorporated in the metal were those physically present in the nebular phases that melted.

The large (factor of 10) range in Ni contents in IAB is remarkable. The low extreme is readily understood by all models as representing the mean composition of the bulk magma, or of a material only slightly fractionated relative to the bulk metal in the precursor material. The very high-Ni contents of Oktibbeha County and San Cristobal were explained by Wasson et al. (1980) as resulting from the melting of FeS and Ni-rich metal that formed when FeS condensation removed Fe from the adjacent metal layer.

Scatter in Trace Elements Among Low-Ni Irons

There is remarkably little scatter in the concentrations of most elements in the set of low-Ni (65–68 mg/g Ni) meteorites. With one or two exceptions, the ratio of the maximum to minimum is ≤1.3 for Co, Cu, Ga, Ge, and Au. The ratio for As is ~1.5, that for W is ~2, and that for Ir is 4. The range for Sb is probably <2, but poorly constrained. That for Re is probably comparable to that for Ir, but less well constrained.

Why is the range for Ir, Re, and W larger than that for the other elements? In the magmatic groups these elements also

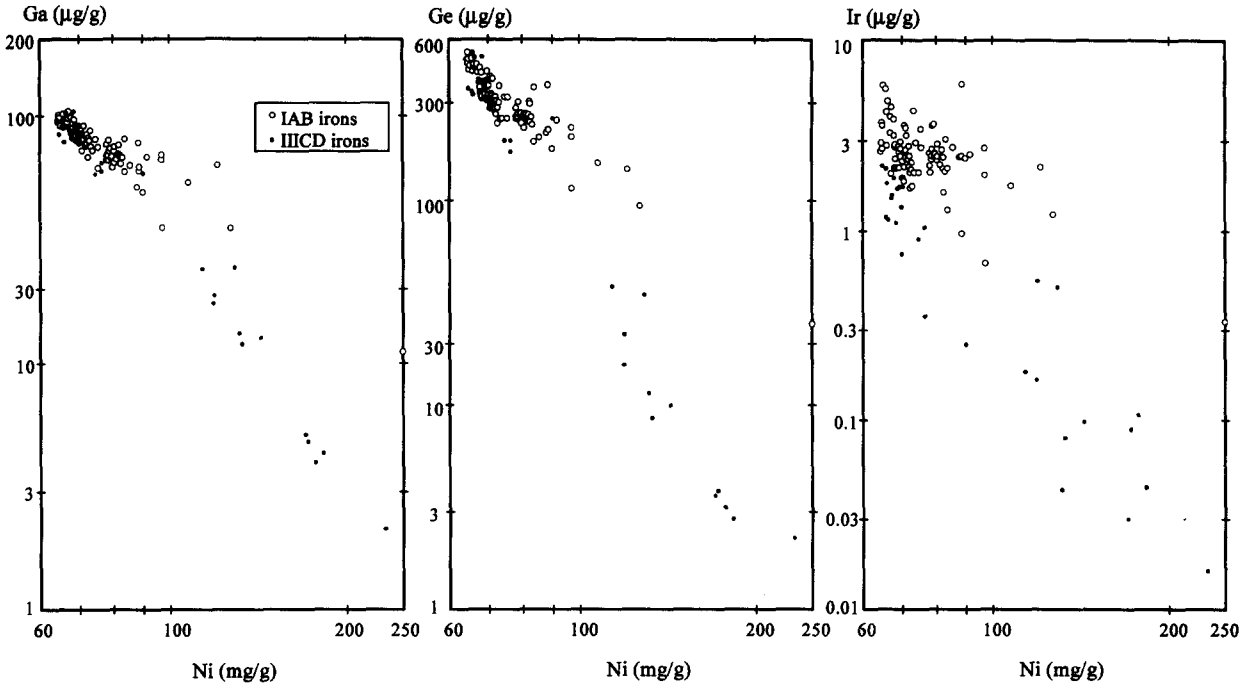

FIG. 5. Log-log Ga-Ni, Ge-Ni and Ir-Ni diagrams for IAB-IIICD meteorites show no hiatus between the meteorites assigned to these categories. In the absence of such a hiatus these taxonomic parameter provide no basis for separating these meteorites into two groups. We recommend that the entire set be treated as a single group, but with the proviso that researchers measuring properties of possible taxonomic value should continue to examine their data to search for hiatus.

show more scatter, and this seems attributable to their high solid/liquid distribution coefficients, which reach values >3 for Ir and Re, and >2 for W. Because the IAB-IIICD melts were S-rich, the distribution coefficients were much larger (Jones and Drake, 1983; Willis and Goldstein, 1982). In the magmatic groups, the scatter probably results from different ratios of cumulus phase to trapped melt. We suggest that the most Ir-rich IAB-IIICD irons formed as cumulus phases.

This has an important bearing on the question of whether IAB (and IIICD) could have formed by fractional crystallization, as proposed by Kracher (1982). The slopes are nearly the same on Ir-Ni and Ge-Ni log-log diagrams, thus, the Ir and Ge distribution coefficients must have been nearly identical. However, if this were the case, the scatter in low-Ni IAB should be nearly the same for Ir and Ge. Nearly identical distribution coefficients may have been present at the cotectic S contents of 290 mg/g, but the difference in these coefficients increases with decreasing S contents (Jones and Drake, 1983). The interpretation of the scatter in low-Ni IAB-IIICD irons as resulting from variations in cumulus-melt ratio is, thus, inconsistent with the requirements of a cotectic fractional crystallization model discussed below.

Detailed Discussion of the Kracher Fractional Crystallization Model

The basic idea of Kracher (1982, 1985) is that fractional crystallization can account for the fractionation trends in IAB-IIICD. Exceptionally large FeS contents in IAB and IIICD magmas led to cotectic crystallization of metal and FeS that generated the low element-Ni slopes observed in IAB.

Kracher followed the canonical view of core formation by separation of a metallic liquid from an internally heated chondritic parent body. Although we shall see that the ideal melt would be a Ni-poor cotectic formed at a temperature of ≈1240 K, Kracher questioned whether phase separation could have occurred in the absence of silicate melting; if only the cotectic formed, the melt fraction may have been as low as 80 mg/g if the S weight fraction was 20–23 mg/g, as observed in ordinary chondrites and in CV, CO, and CK chondrites (Wasson and Kallemeyn, 1988). Higher S contents as observed in EH, EL, and CR-an Al Rais, and would be present in anhydrous and reduced chondrites having CM- and CI-like bulk compositions would lead to melt fractions of 150–240 mg/g, an amount that might be great enough to allow segregation of a low-viscosity melt.

Kracher also noted that it might be necessary to incipiently melt silicates in order to lower the interfacial tension. He, therefore, suggested that the temperatures reached the silicate solidus at ≈1370 K, at which a plagioclase melt formed, and more metal dissolved making the volume fraction of metal-sulfide melt substantially larger than at the cotectic. Melt extraction at appreciably higher temperatures was not considered plausible because these would cause extensive silicate melting inconsistent with the chondritic compositions of IAB silicates (Kracher, 1982).

At the FeS-metal cotectic the weight fraction of FeS in the crystallizing solid is ≈0.84. Kracher noted that, because the distribution coefficients for most siderophiles are very low in FeS, the crystallization of a melt more metal-rich then the cotectic would lead to kinks in element-Ni log-log diagrams

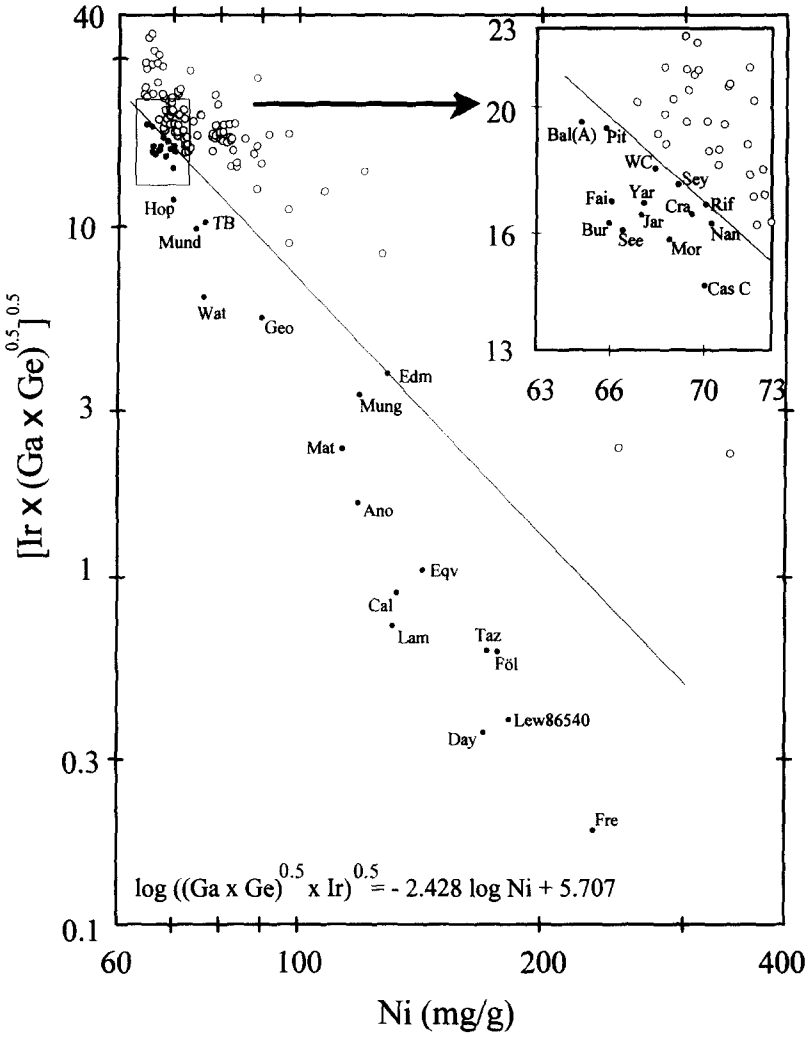

FIG. 6. We plotted the log of a geometric mean of Ga, Ge and Ir [(log Ga + log Ge + 2·log Ir)/4] against log Ni in order to devise a basis for separating IAB-IIICD into IAB and IIICD portions. As shown by the insert, there is no hiatus between the two populations at Ni contents <73 mg/g.

at the point that metal crystallization brought the composition of the magma to the cotectic composition.

We tested the Kracher model by using metal/melt distribution coefficients determined for S-rich compositions (Willis and Goldstein, 1982; Jones and Drake, 1983). For simplicity, we did not attempt to include the effects of P and C, although these would also have played important roles in an actual fractional crystallization model. Our purpose was mainly to examine whether the general trends could be generated, not to produce a quantitative explanation of the trends.

The effect of S on the distribution coefficients of Ga, Ge, and Ir is so sensitive to the S content that we cannot use constant coefficients during the approach to the cotectic composition. When the crystallization follows the cotectic trough, the change in the S content is relatively minor (Kullerud et al., 1969), and it seems a reasonable assumption that distribution coefficients remained approximately constant for the remainder of the crystallization process. We used a S content of 290 mg/g at the onset of cotectic crystallization process; this compares with a value of ≈310 mg/g at the Fe–FeS join and 220 mg/g S at the Ni-NiS join (Kullerud et al., 1969).

Figure 8 shows Ga-Ni trends calculated for this fractional crystallization model; the relevant equations are those summarized by Kracher (1982). We found that a liquid core having an initial temperature of 1370 K and an initial S content of 250 mg/g reached the cotectic when the fraction of melt solidified was about 0.15. We chose initial Ni and trace element concentrations that yielded the low-Ni extreme of IAB at the onset of cotectic crystallization; for Fig. 8 the values were 46 mg/g Ni and 41 μg/g Ga.

We used the distribution-coefficient relationships given by Jones and Drake (1983) for Ni and siderophiles other than Ga; in most cases these are similar to the values of Willis and Goldstein (1982). These experimental data were reviewed by Jones and Malvin (1990) and Haack and Scott (1993). For the distribution coefficient of Ga, we used the revised regression expression given by Haack and Scott (1993), which corrects an error found in the Jones and Drake (1983) dataset. As examples, metal/melt distribution coefficients of Ni and Ga increase from 1.36 to 1.51 and from 6.6 to 9.0, respectively, as the S content in the liquid increases from 250 mg/g to 290 mg/g. A key question is the FeS/melt distribution

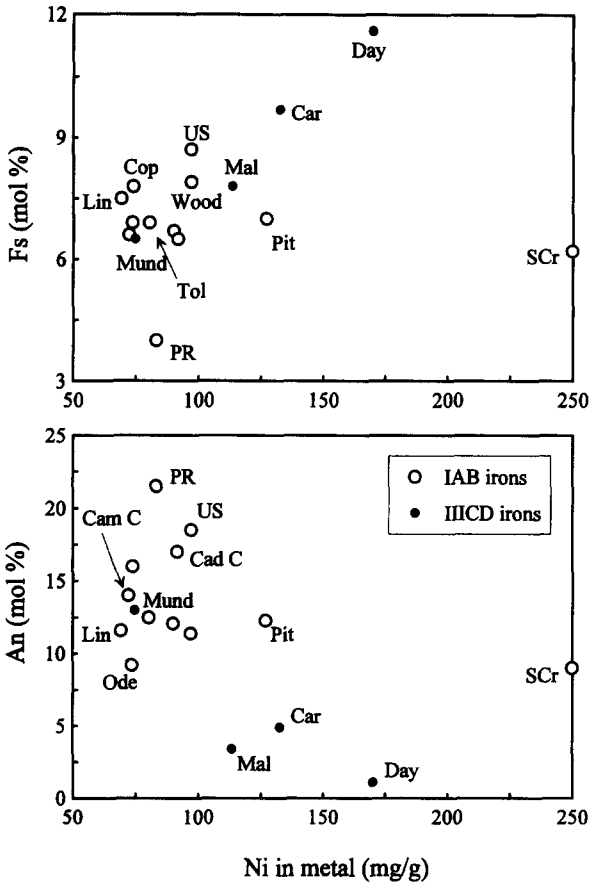

FIG. 7. As pointed out by McCoy et al. (1993), silicate mineral compositions in IAB irons tend to have small ranges and to show no correlation with the Ni content of the metal. In contrast, pyroxene compositions in IIICD Carlton and Dayton fall outside the IIICD range, and there is a positive correlation with Ni within the IIICD set. Plagioclase An contents in three IIICD irons fall outside the IAB range. As stated in the text, we question the taxonomic value of these observations. See Fig. 3 for the sources of data. Caddo County from Takeda et al. (1994).

coefficient to use in these calculations. We first assumed a value of 0.02 (i.e., effectively zero), then used a higher value if required to obtain an appreciably better fit (e.g., in order to make the calculated trend fit the observed IAB trend, we chose 0.6 as the distribution coefficient for Ga in FeS). We also show the curve calculated for $D_{Ga,FeS} = 0$ on Fig. 8. An alternative means to fit the IAB trend is to use values of $D_{Ga,met}$ about 30% greater than obtained from the Jones-Drake relationship and increase the initial Ga by a comparable degree.

To model the IIICD trend, both the distribution coefficient and the initial concentration of Ga had to be increased by a factor of 2 relative to those used for the IAB trend. We have not been able to find alternative ways to explain the differences between IAB and IIICD within the constraints of the Kracher model. Thus, if fractional crystallization of independent cotectic liquids is responsible for the IAB and IIICD trends, the great similarity between low-Ni IAB and IIICD irons must be considered fortuitous.

Our calculations (Fig. 8) also show the kink noted by Kracher (1982) for magmas having initial compositions undersaturated in FeS. In fact, there are no iron meteorites having the extremely high Ga and Ge contents calculated for the first metal crystallized from such a Kracher-type model (a few Ir-rich IAB-like irons are known). This constitutes a strong argument against the model as formulated. Of course, if the starting composition was nearly cotectic, IAB and IIICD irons having very high Ga, Ge, etc. would not have been produced but, as noted by Kracher (1985), it is doubtful that phase separation to form a large magma body could have occurred if temperatures never exceeded 1240 K.

We conclude from the absence of IAB irons having the predicted high Ga, Ge, and Ir contents that the IAB irons cannot have been formed by fractional crystallization of a melt having a metal-rich initial composition requiring >10% metal crystallization prior to reaching the cotectic composition. We, therefore, limited our further consideration to models in which the initial melt composition is exactly at a cotectic composition that can crystallize initial solids having compositions at the low-Ni extreme of IAB-IIICD. In Fig. 9, we show four element-Ni trends calculated for a melt having an initial composition on the cotectic near the Fe–FeS join. Distribution coefficient data for the other interesting elements Co, Cu, As, and Sb are not available. The $D_{X,FeS}$ values that differ from zero are listed on Fig. 9. It should be noted that the cotectic temperature drops from ~1240 K in liquids having −40 mg/g Ni to −1170 K at Ni contents of 190 mg/g; the viscosity undoubtedly also increases.

Figure 9 shows that IAB-like slopes are obtained from distribution coefficients relatively close to those determined by Jones and Drake (1983) and Willis and Goldstein (1982), assuming that S content in liquid is 290 mg/g. We were able to generate good fits from all distribution coefficient data (except the $D_{Ir,met}$ and $D_{Ge,met}$ data of Jones and Drake, 1983) by assigning moderate values to $D_{X,FeS}$; equally good fits could have been obtained by increasing $D_{X,met}$ values. We found it

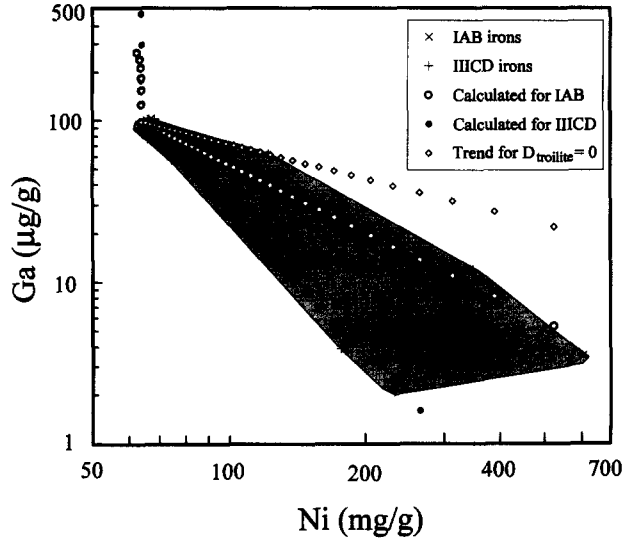

FIG. 8. The cotectic fractional crystallization model of Kracher (1982) was fitted to IAB and IIICD Ga-Ni trends by using three different sets of partition coefficients mainly based on data by Jones and Drake (1983); the steep initial trend reflects metal crystallization leading toward the cotectic composition. In each case, the model predicts high Ga values that are not observed (the diamonds and open circles superimpose). See text for details.

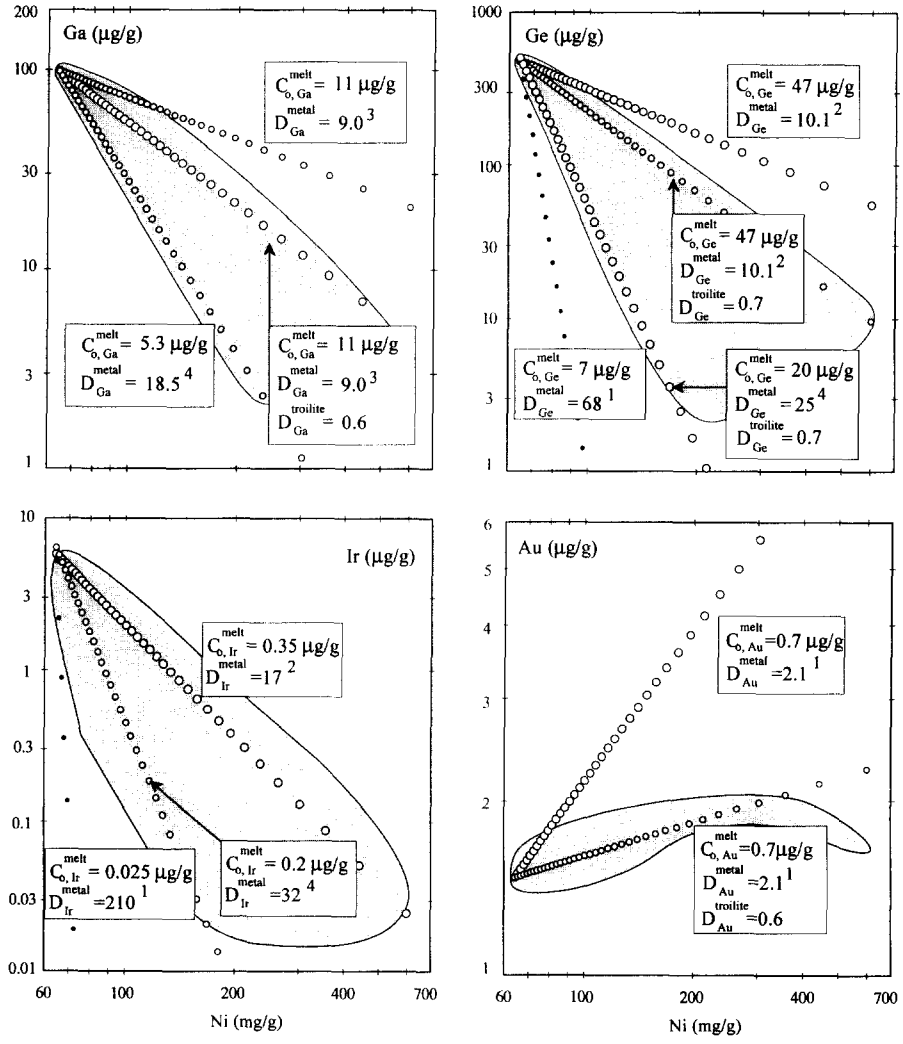

FIG. 9. Trends produced by fractional crystallization of a metal-troilite cotectic on Ga-Ni, Ge-Ni, Ir-Ni, and Au-Ni diagrams. Metal/melt distribution coefficients are from Jones and Drake (1983) and Willis and Goldstein (1982); FeS/melt distributions are assumed to be zero: A second trend involving a higher D_{FeS} is shown for those cases where this yields an appreciably better fit to the IAB trends. Superscripts on distribution coefficients represent data sources; 1: Jones and Drake (1983), 2: Willis and Goldstein (1982), 3: Haack and Scott (1993), and 4: our fit for IIICD trends.

necessary to use the $D_{Ir,met}$ and $D_{Ge,met}$ values appreciably lower than those of Jones and Drake (1983), which yielded slopes too steep to fit IAB or IIICD.

Despite the success in emulating IAB trends, there remains a major way in which a single-magma cotectic model fails; it predicts far more high-Ni irons than are actually observed. In Fig. 10, we show that the cotectic model predicts a quite moderate decrease in abundance with increasing Ni content, whereas the actual IAB and IAB-IIICD distributions have abundances that fall rapidly. Further, the observed distributions should be weighted on the basis of the recovered mass which is, on average, perhaps ten times larger for irons with Ni $<$ 85 mg/g than for irons with Ni $>$ 150 mg/g. This comparison effectively rules out models calling for IAB formation by efficient fractional crystallization in a single core having a Ni-poor cotectic initial composition. A caveat is that our museum collections are somewhat biased in favor of large iron finds. Although attrition in space would be expected to be more destructive of irons with higher FeS contents, this should not introduce a bias if the entire group formed by cotectic crystallization. Complex models involving trapped melt might lead to inefficient crystallization and thus be more successful at duplicating the Ni distribution. Inefficient cotectic crystallization of a series of impact melt pools differing in their Ni contents is discussed in connection with our impact model.

There are other reasons to reject IAB-IIICD models calling for the fractional crystallization of large magma bodies, mostly related to the presence of abundant chondritic silicates containing large amounts of planetary-type rare gases and excess ^{129}Xe, indicating early cooling to a temperature low enough to allow Xe retention. Fractional crystallization can only occur if the magma is well stirred. On an asteroid-size body, this requires a relatively low viscosity. We have not yet found information about the viscosity of the cotectic melt, but it seems that any viscosity low enough to allow repeated overturning of the residual melt would thoroughly remove any silicates that happen to have been introduced into the melt.

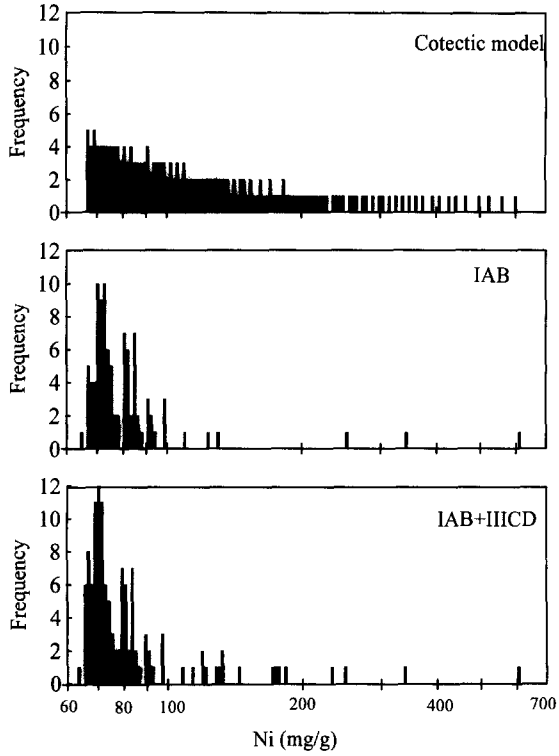

FIG. 10. The cotectic model predicts far more high-Ni irons than are observed in IAB or IAB-IIICD. The upper diagram shows the distribution predicted by the cotectic model, the two lower diagrams the distributions actually observed. The disagreement with predictions would be still more pronounced if one weighted the observed distributions by the recovered masses.

Particularly relevant are the large, cm-size silicate clasts, since Stokes' law ascension velocities increase linearly with diameter. Kracher (1985) recognized this problem and suggested that the presence of silicate clasts required the injection of residual magma into silicates, but noted that this implies that the trapped magma should have very large S contents (we above estimated 290 mg/g); such high-S contents are not found in silicate-rich IAB sections (such as the El Taco section described by Wlotzka and Jarosewich, 1977), where there seems to be no doubt that they should have survived space weathering and passage through the Earth's atmosphere. An additional problem is that, if the earliest crystallized solids formed a shell on the outside of the core, these would have tended to shield the hypothesized chondritic "mantle" from the injection of highly evolved magmas such as that represented by San Cristobal, with 250 mg/g Ni. In fact, crystallization of a core having a cotectic composition would be expected to produce a thick FeS-rich layer at the core-mantle boundary.

As discussed already by Wasson (1972), the thermal history of the IAB parent body seems to have been very different from that of the magmatic bodies. The largest precursor γ-iron crystals in IIIAB reach dimensions of at least 2 m. In contrast, although IAB irons cooled through the $\alpha + \gamma$ field (700–1000 K) at about the same rate as the IIIAB irons, the maximum dimensions of γ-iron crystals in IAB are about 0.5 m. This implies that the IAB parental region transited the temperature range 1200–1600 K where γ-iron crystals were growing many times faster than the IIIAB parental region. Rapid cooling makes efficient fractional crystallization less likely. Slow cooling is needed to maximize elemental exchange between the magma and the fractionated boundary layer adjacent to the freshly crystallized solid.

In summary, there is strong evidence against a model calling for the formation of IAB-IIICD (or the IAB portion of this group) by the efficient fractional crystallization of a single magma body having a cotectic composition. The crystallization of a cotectic magma can generate large Ni ranges that lead to low slopes on element-Ni diagrams, but such a model cannot account for the observed distribution of Ni contents or the presence of large chondritic clasts in IAB.

AN IMPACT MODEL THAT INCLUDES MAGMA MIXING AND CRYSTAL SETTLING

Evidence Regarding Impact Models

Wasson et al. (1980) proposed an impact melt model for IAB-IIICD; they explained the element-Ni trends in terms of differing degrees of melt extraction of volatile Ga and Ge and refractory Ir, Re, and W from primordial sites in the oxide components of unequilibrated chondritic materials. The higher the temperature of the impact melt, the more efficient the extraction. Irons having high-Ni contents were interpreted to have formed of metal depleted in Fe by FeS formation. The greater the melt temperature, the higher the degree of dilution of such Ni-rich metal by low-Ni metal from the interiors of precursor metal gains.

The reasons for favoring an impact-melt model for IAB are the following. (1) Silicates are common in many IAB irons and may be present in all. Melt viscosities low enough to allow multiple overturns of the magma during fractional crystallization would inevitably have led to silicate removal from the magma. Impact processes can lead to very brief periods of low viscosity, thus accounting for incomplete segregation of melt from unmelted solids. (2) IAB silicates are essentially chondritic in composition and have moderately large amounts of primordial ^{36}Ar and ^{132}Xe. As observed in chondrite breccias, impact heating and shearing can mobilize metal and troilite while leaving nearby silicates essentially unmelted; in contrast, the slow, shear-free heating inherent in heating by internal sources requires appreciably higher mean temperatures in order to achieve metal-silicate segregation and would probably lead to widespread separation of a plagioclase-rich melt from the silicates, and extensive outgassing of the residual silicates. (3) I-Xe formation intervals for IAB silicates increase with increasing mean Ni content of the metal. Magmatic models have difficulties accounting for this observation (Kracher, 1985), whereas Wasson et al. (1980) note that it would be a natural result if the continuing impact alteration of a megaregolith on average led to generation-n + 1 melts having lower Ni contents than generation-n melts. (4) Because the solubility of FeS in metal is very low (<1%; Buchwald, 1975) the large abundance of troilite in most IAB-IIICD irons requires large amounts of trapped liquid, consistent with rapid solidification of impact generated melt, but less easily explained by a slowly crystallizing magma. These troilite nodules are more or less uniformly distributed on scales ≥20 cm.

McCoy et al. (1993) noted that the impact model does not appear to have been general; no similar irons are known for the ordinary chondrite bodies. This suggests that, relative to ordinary chondrites, the IAB precursor materials were more easily melted (more rich in FeS, had higher porosities) and possibly also that mean interparticle (i.e., impact) velocities were higher at the time and place the IAB body evolved relative to those associated with the formation of ordinary chondrites.

Mixing of Impact-Generated Melts

If we are correct that the absence of a hiatus between the irons in the IAB trend and the IIICD trend indicates that these irons should all be assigned to the same group, it is necessary to explain why the range of groups in Ga, Ge, and Ir increases (i.e., the vertical spread on Fig. 5 increases) with increasing Ni content. We suggest that mixing of primary (possibly impact-generated) magmas offers a reasonable solution. Element-Ni trends that yield steep negative slopes on log-log diagrams give strongly curved arrays if magmas are mixed.

In Fig. 11, we illustrate the effects of mixing on the Ga-Ni diagram. To calculate this diagram, it was necessary to assume that the IIICD side of the IAB-IIICD field was the primary side, and that the remainder of the field formed by mixing these primary magmas.

The simplest assumption is that the primary IIICD trend is linear. The major problem of such a model is to form Oktibbeha County with a Ni concentration of 610 mg/g. This requires extrapolation of the IIICD trend down to extremely low Ga, Ge, and Ir values at a Ni concentration of ~630 mg/g; the extrapolated Ga value would be 0.1 μg/g, those for Ge and Ir much lower still. If the primary melts formed by impacts, as Wasson et al. (1980) proposed, this requires a remarkable sequestering of these three elements in unmelted phases. A more plausible variant of the impact model is that the slope of the locus of primary melts became less steep at Ni contents below ~240 mg/g (e.g., at Ga contents near 3 μg/g) and thus, that the Ga, Ge, and Ir content of Oktibbeha County are only slightly higher than that of the primary melt. As noted below, an alternative to mixing is that modest amounts of crystallization occurred in the small (perhaps a few cm or a few tens of cm) Ni-rich IAB impact-melt pools, and that Oktibbeha County is a cumulus solid of a Ni-rich pool.

Crystallization Effects in Impact Melt Pools

We showed above that the fractional crystallization of FeS-saturated melts seems well suited to account for the low slopes on Ga-Ni, Ge-Ni, and Ir-Ni diagrams, and that this model leads to Ni contents in late-crystallized solids that can be much higher than those in early-crystallized solids. In fact, a major reason to reject that model for explaining all IAB irons in a single magma is that it yields too large a fraction of high-Ni irons.

We propose that moderate amounts of (probably inefficient) crystallization could have occurred in relatively small (ca. 1 m size) impact-generated melt pools, and that this may be responsible for some fraction of the observed element-Ni

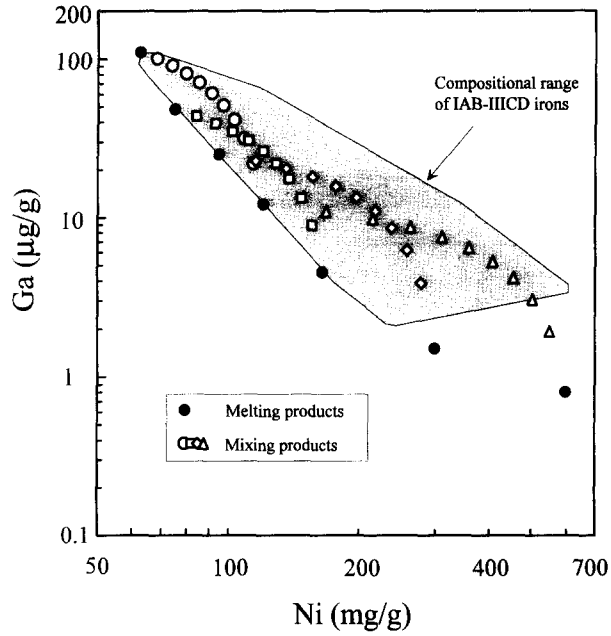

FIG. 11. The entire Ga-Ni IAB-IIICD trend can be accounted for by a mixing model. It is hypothesized that primary impact-generated partial melts form an array corresponding to the lower (IIICD) envelope of the IAB-IIICD field (open circles). Mixing of these melts are shown by filled symbols with different shadings. Each symbol corresponds to a change in 0.1 in the mixing fraction.

trends. Slow crystallization and crystal settling seems particularly likely in melt pools having Ni > 190 mg/g and T_{cot} < 1170 K since these temperatures may have been comparable to those in the surrounding megaregolith, and thus, cooling rates may have been low enough to prevent rapid solidification. The advantages of this impact model relative to models calling for the crystallization of large magma bodies are: (1) impact heating is better able to preserve the chondritic compositions and high primordial-gas contents of the silicates; and (2) even though silicates would have been separated from those metal-FeS magmas that experienced crystal settling, the separation distances would have been small, and subsequent impacts could have introduced silicates into metal having a wide range of compositions.

Our new model differs only in details from the Wasson et al. (1980) model. We retain the idea that there was a wide range of temperature-related initial compositions among the impact-melt pools and we consider it probable that the low-Ni melts had temperatures appreciably above that of the cotectic, mainly because we doubt that viscosities would be low enough to produce sizable (>10-m size) metal pools at the cotectic temperature, as seems required to explain the uniformity in composition of Canyon Diablo irons, some of which were probably separated by distances >40 m (Wasson and Ouyang, 1990). We suggest that most melt pools chilled without appreciable fractionation beyond the occasional presence of m-size cumulates. We now suggest that a few Ni-rich pools experienced crystal settling, leading to a general increase in the compositional spread. It seems particularly probable that crystal growth was responsible for the formation of irons having high Ni contents, perhaps those with Ni ≥ 300 mg/g. We

agree that crystal settling requires relatively low-cooling rates of the cotectic magmas. The ca. 50-cm dimensions of the parental gamma crystals in IAB irons also require slow cooling in a temperature interval just below the cotectic temperature. Wasson et al. (1980) suggested that low cooling rates in a megaregolith indicated that a heat source, perhaps impact heating, was present during this period.

Cooling Rates and Formation Models

Cooling rates of iron meteorites can be estimated from taenite Ni profiles or central Ni contents. A somewhat less precise method is based on the widths of kamacite bands. Herpfer et al. (1994) compared observations of central taenite Ni contents in IAB chondritic inclusions and in the host metal. In irons with Ni < 145 mg/g, they observed cooling rates of 25–70 K Ma^{-1}, with some tendency to increase with increasing Ni content at Ni > 90 mg/g. The cooling rate of San Cristobal, with 250 mg/g Ni the only iron in the set with Ni > 145 mg/g, was estimated to be 200 K Ma^{-1}, but four taenite Ni values yielded apparent rates ranging from ~25 to ~1000 K Ma^{-1}. These results contrast with band-width-based estimates by Rasmussen (1989), which show roughly the same range but show no tendency to increase with increasing Ni. These studies can be summarized to indicate near-constant rates with a possible tendency to increase with increasing Ni content.

Core models such as that of Kracher (1985) predict cooling rates that are independent of Ni content. The simplest version of the impact melt-pool model predicts an appreciable range of rates, also with no correlation with Ni content. If, however, the impact model is made slightly more complex by covering the melt-pool–bearing megaregolith with a fine-grained, porous, insulating regolith (Rasmussen, 1989), the range in predicted cooling rates is greatly reduced. Thus, the inferred IAB cooling rates offer little basis for choosing between core and impact models of their origin.

Finally, we note that published cooling rates are model dependent; the observed taenite Ni profiles can be generated by annealing at constant low temperature or at fluctuating temperatures, as would be expected in the megaregolith of a growing body. Thus, no depth information can be obtained from studies of metal that was annealed in a regolithic setting.

RELATIONSHIP BETWEEN IAB-IIICD AND THE CARBONACEOUS CHONDRITES AND THE GERMANIUM AND GALLIUM FRACTIONATION WITHIN IAB-IIICD

As discussed in the previous section, generation of the Ga–Ni and Ge–Ni trends by differing degrees of impact melting probably requires that Ga and Ge were present as oxides in the chondritic precursors of IAB-IIICD metal. In an earlier section, we noted that the silicate oxygen-isotope data shown in Fig. 3 imply a possible relationship with the carbonaceous chondrites. In this section, we examine possible relationships with the carbonaceous chondrites, then return to the question of the nebular condensation of Ge and Ga.

According to the impact model, the compositions of low-Ni IAB irons provide an estimate of siderophile abundances in the precursor materials. This is approximately true of the fractional crystallization model as well; the bulk magma is thought to be roughly representative of the abundances in the precursor materials, and the compositions of the most Ni-poor IAB members are then fractionated from this composition by the magnitude of the partition coefficients. The mean composition of IAB-IIICD irons in the Ni range 65–68 mg/g is listed at the bottom of Table 1.

In Fig. 12, we compare CI and Ni-normalized volatile-element abundance ratios in IAB-IIICD with those in chondrite groups having high (e.g., CI, CM, EH) and low (e.g., CV, CO, CR, H, L, LL) volatile abundances. Of particular note are the low volatile abundances in Renazzo and other "normal" CR chondrites having oxygen-isotope compositions quite close to IAB silicates. This renders improbable a close link between IAB and CR.

The abundances of Co, Ga, Ge, and Au in low-Ni IAB-IIICD irons are quite high, in the range 1.5–2. Depressed ratios well below the CI value are observed for Cu and Sb. Other elements including Ir and As show ratios within about a factor of 1.1 of the CI line.

As discussed by Willis (1980), all iron meteorite groups have low Cu abundance ratios. In the case of IAB-IIICD, there are four possible explanations for low Cu: (1) incomplete condensation from the nebula; (2) incomplete extraction from the (chondritic) precursor solids; (3) preferential extraction of Cu into an early melt; and (4) unrepresentative sampling of Cu-rich phases associated with the metal.

We reject incomplete condensation because IAB contains high abundances of other volatiles having similar nebular condensation temperatures (see, e.g., Wai and Wasson, 1977). It is, therefore, likely that Cu was efficiently condensed into the chondritic precursor materials. There also seems little reason to doubt that Cu was completely extracted from the precursor solids. It probably condensed from the nebula as metal or a sulfide as opposed to a refractory oxide that failed to melt.

During the formation of magmatic groups, Cu may have been extracted into an early FeS-rich melt that failed to equilibrate with later metallic melts that crystallized to form the

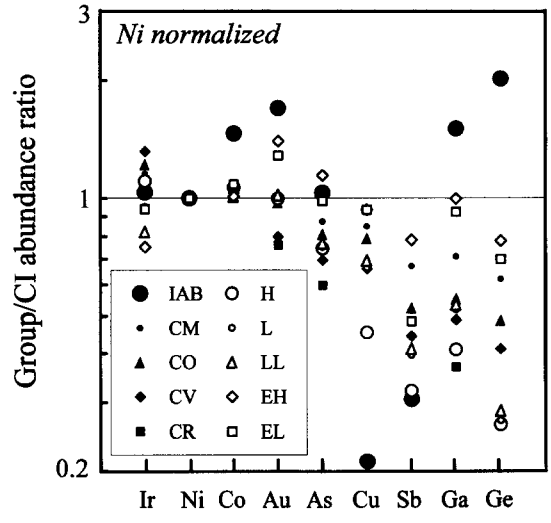

FIG. 12. Comparison of Ni-normalized volatile-element abundances in low-Ni members of IAB-IIICD with those in several chondrite groups (CR data from Kallemeyn et al., 1994; others from Wasson and Kallemeyn, 1988). See text for details.

iron meteorites (Kracher and Wasson, 1982). Because there is abundant evidence that the IAB irons formed as FeS-rich melts, loss by this mechanism seems unlikely.

We suggest that unrepresentative sampling is the correct explanation for the low Cu content in IAB. Although trends in magmatic groups show low positive or negative slopes implying $D_{Cu,met}$ values near unity, in S-rich magmas such as IAB it seems probable that Cu forms S complexes in the melt that lead to low $D_{Cu,met}$ values. If values are as low as 0.1–0.2, the Cu would tend to remain in the trapped-melt pockets during IAB crystallization. We suggest that this Cu eventually formed native Cu (and possibly a Cu-rich sulfide) that was rarely sampled in our procedure.

We suspect that unrepresentative sampling is also the explanation for the low Sb abundance ratio. As with Cu, perhaps one sample in 20 is $\geq 2\times$ higher than others from the same meteorite, in support of the idea that the missing Sb is in rare, generally unsampled phases.

Enhanced *X*/Ni Ratios of Gallium, Germanium, Gold, and Cobalt

Although crystallization would produce enhanced ratios for elements strongly partitioned into the metallic solids, this can only account for the high Ga and Ge ratios, not those of Au and Co. Also, Ir, which together with Ge shows the largest $D_{X,met}$ values, does not show an enhanced abundance ratio. We conclude that solid-liquid partitioning has played at most a minor role in producing the observed abundance ratios.

There are two ways that the volatility could be responsible for high Au, Ga, and Ge abundance ratios: (1) metamorphism-induced vapor-phase transport could have led to a redistribution of planetary volatiles out of chondritic matter into metallic magmas; or (2) nebular processes could have produced chondritic materials having high abundance ratios.

Although, granted the appropriate composition of the ambient gas, Ga, Ge, and Au are all capable of forming volatile compounds at metamorphic temperatures, this process could be hardly be responsible for their high abundance ratios in low-Ni members of IAB. A large magma body would require miraculous plumbing in order to efficiently transport these elements through the vapor from unmelted chondritic material into the magma (rather than through cracks to the surface regions of the planet). In the impact model for IAB formation, one would need to produce large degrees of transport during the brief periods of impact heating. However, the fraction of volatiles associated with the veins in brecciated chondrites is generally minor, and there is no reason to believe that such transport could uniformly increase volatile/Ni ratios by factors of 1.5, relative to those in the chondritic precursors. Also, if vapor transport were an important process, it may have been difficult to avoid contamination of melt pools having very low contents of Ge and Ga.

Wasson et al. (1980) noted that Ni is more refractory than Fe, and that incomplete melting of nebular metal grains might be responsible for abundance ratios >1. However, we find no reason to believe that all Ni-bearing metal was not melted, and this mechanism cannot explain why the Ge/Ni ratio is so much larger than the Ga/Ni ratio.

Nebular volatility offers better solutions. Differences in the volatile contents of chondrites attest to the possibilities of volatile redistribution during nebular-agglomeration. The standard cosmochemical picture is that the starting nebular composition was CI-like at all locations, i.e., that complete condensation and efficient accretion would have produced chondrites with CI-like compositions. A trivial way to explain high IAB volatiles is to assume that this model did not apply at the IAB location, but that this part of the nebula was enriched in Ga, Ge, Au, Co, etc. We cannot exclude this model, but it seems better to try to explain the observations within the constraints of the standard cosmochemical model.

A plausible nebular-agglomeration model that could lead to high volatile/refractory ratios of siderophiles in the chondritic precursors of IAB involves an enhanced accretion of fine-grained materials having high surface areas. Such a process may be responsible for the observation that volatile-element abundances in chondrite groups (e.g., CM, H, L) decrease with increasing elemental volatility (Wai and Wasson, 1977). The chief difference between CM and CO chondrites seems to be that the CM chondrites have an appreciably higher abundance of a fine, volatile-rich "matrix" component. It is hardly far-fetched to suggest that the IAB precursor chondrites could have formed from materials that were moderately enhanced in a fine nebular component that carried several volatiles (such as Ga, Ge, Au, and possibly C and S) compared to other chondritic materials forming earlier at the same place.

We noted above that Ga and Ge were probably present as oxides in the precursor materials. Wasson and Wai (1976) and Wai and Wasson (1979) showed that Ga and Ge tend to condense as oxides in low-pressure ($pH_2 \sim 10^{-6}$ atm) nebular environments. In higher pressure nebulae, a similar tendency to form oxides could result if kinetic factors, perhaps associated with high nebula cooling rates, made it difficult for these elements to diffuse into preexisting metal grains.

A variant of this model also offers an explanation for the high Au/Ni ratios. Volatile Au might have been enriched in a fine metal component if it was unable to diffuse into the common coarse metal. Its enhanced abundance relative to As would require that an appreciable fraction of As was not in the hypothetical fine component. At lower temperatures, S would have condensed on this fine metal, and would probably have converted the Fe almost entirely to FeS. Interestingly, this FeS would not have entered the lowest-temperature impact melts because no Fe-rich metal would have been present to form the eutectic.

Because the condensation temperature of Ni is slightly greater than that of Fe and that of Co slightly lower, it is conceivable that a fine component might have an elevated Co/Ni ratio, but it is difficult to envision that the mass of Co in such a component could be great enough to increase the bulk Co/Ni of the low-Ni IAB precursor enough to produce the observed $1.5\times$ enhancement relative to CI.

In summary, consideration of alternative models shows that planetary processes above cannot readily explain the high element/Ni abundance ratios of Co, Ga, Ge, and Ir. Instead, the enhancements appear to reflect nebular processes. The Ga, Ge, and possibly the Au appear to have condensed in a fine nebular component that was slightly enriched in the precursor chondritic materials. The high Co/Ni ratio may partly reflect

such processes, but other processes not considered by us seem also to have played a role.

COMPARISON OF IAB-IIICD WITH THE OTHER NONMAGMATIC GROUP IIE

The only other group that has been designated nonmagmatic is group IIE (Wasson and Wang, 1986). These irons share with group IAB-IIICD the relatively low slopes on element-Ni diagrams. Silicate inclusions are found in about half the IIE members. With the exception of the IIE-an iron Netschaevo (Bild and Wasson, 1977), these silicates are not chondritic. However, their compositions are generally consistent with formation from chondritic precursors by simple processes (e.g., extraction of a low-temperature melt). A summary of silicate properties is given in the recent paper by Olsen et al. (1994), who described a very large silicate in the Watson iron having H-chondrite composition minus metal and FeS.

In Fig. 13, the trends in the metal of group IIE irons are compared with those in IAB-IIICD, and with magmatic group IIIAB. There are important similarities and differences between IIE and IIICD. Similar are the generally low slopes on plots of refractory siderophiles vs. Ni and the relatively high positive slopes on the Cu-Ni diagrams. Different are the much smaller Ni range in IIE and the high slopes on As-Ni and Au-Ni diagrams. The latter are only slightly lower than those in magmatic group IIIAB, but the total As and Au ranges are considerably smaller.

In several of the IIE irons (e.g., Colomera, Weekeroo Station) the silicates form curved globules, suggesting that they briefly existed as a melt in a system that was quenched soon after an impact-mixing event. In Colomera, a large crystal of sanidine is present that seems to have been formed by vapor-phase transport. Contents of primordial rare gases are low in IIE, thus, they seem to have experienced more extensive outgassing at high temperatures than those in IAB irons. One IIE iron (Kodaikanal) seems to have had the original medium-octahedrite structure replaced by a fine-octahedrite structure; a late (3.8 Ga ago—Burnett and Wasserburg, 1967) impact heating event may have been responsible for resetting the age and the alteration of the original structure.

In contrast to IAB, IIE irons contain no carbides and substantially smaller fractions of FeS. As summarized by Olsen et al. (1994), the silicates in Watson appear to consist of slightly altered H-chondrite materials, implying low H-like (ca. 20 mg/g) bulk S contents. These differences may be the key to differences in group properties and trends. If the IIE parental materials had much lower FeS contents, the generation and segregation of melt bodies would have required appreciably higher temperatures, and thus, melt-generating impact events would have produced more pronounced metamorphic effects, including greater loss of primordial rare gas. A lower FeS content in the parental chondritic material could also be responsible for the fact that element-Ni slopes tend to show more "magmatic" character than those in IAB-IIICD.

In summary, the differences in properties between IIE and IAB-IIICD appear to be consistent with both having formed from impact-generated melts, the observed differences mainly reflecting the lower FeS contents of the IIE melts and the higher initial temperatures of these melts.

SUMMARY

Formation of Nonmagmatic Iron Meteorites

There are two major differences between magmatic and nonmagmatic groups: their slopes of metal compositional trends are generally different, and the nonmagmatic groups contain silicates having chondritic compositions or compositions that can be produced by the extraction of low-melting phases from chondritic materials. Planetary-type rare gases are present in the nonmagmatic groups (mainly in the silicates), but absent in the magmatic groups.

An especially noteworthy compositional difference is the observed in log-log Ir-Ni trends, for which the slopes in magmatic groups range from -20 to -40, whereas those in the nonmagmatic groups are -5 if IIICD is treated as a separate group, but > -4 in combined IAB-IIICD and in IIE. On log-log Ga-Ni and Ge-Ni diagrams magmatic groups show small ranges and slopes near zero, whereas in IAB slopes are in the range -4 to -5. In IIE, the combination of a small Ni range and considerable scatter make it difficult to define the slopes.

Although the nonmagmatic groups IAB and IIE share several properties that distinguish them from the magmatic groups, they differ in important ways. The difference in silicate compositions was already noted. Group IIE metal has a much smaller range of Ni contents and shows somewhat different element/Ni slopes for some elements. There is good reason to believe that IIE irons formed by the impact melting of H-chondrite-like material having low ($\sim$20 mg/g) FeS contents; the chondritic precursors of the IAB irons had much higher FeS contents and, as a result, melts extensive enough to segregate as melt pools could be formed at much lower temperatures.

Kracher (1982, 1985) suggested that IAB and IIICD formed by fractional crystallization of two or more FeS-rich magma bodies. We modeled this crystallization using the distribution coefficients of Jones and Drake (1983) and Willis and Goldstein (1982), and found that crystallization of a cotectic melt provides a reasonably good match to the observed IAB trends. We find, however, that this model cannot reproduce the observed Ni distribution in IAB; the median Ni content of IAB-IIICD is 73 mg/g, whereas that calculated for the single-magma fractional-crystallization model yields is 103 mg/g. A proper weighting to allow for the larger preatmospheric masses of low-Ni irons would lead to a still lower IAB median Ni content.

An even stronger reason to reject a model calling for IAB formation in a single magma (and IIICD in a second magma) is the presence of chondritic silicates; a convecting magma will rid itself of silicates within a short period compared to the crystallization lifetime. If the dimensions of the magma chamber were large ($>$1 km), it is highly unlikely that silicates would have been reintroduced into a large fraction of the irons produced in this magma.

There are several problems with single-magma IAB models if the heat source is internal, e.g., resulted from the decay of short-lived nuclides. Because there is no shear in these models, they must achieve higher temperatures in order to segregate the FeS-rich magma from the silicate host. The higher the temperature, the greater the loss of planetary gas from the silicates, and the less likely that the large amounts of melt

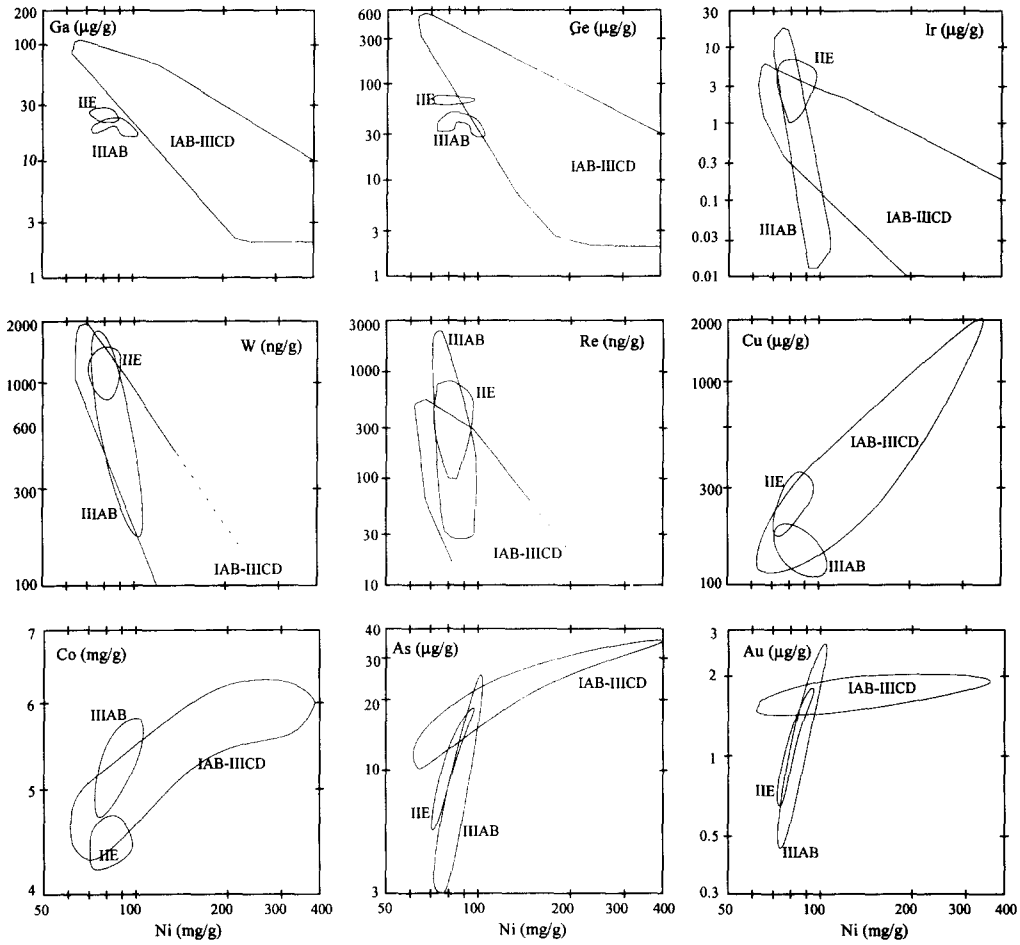

FIG. 13. Comparison of trends in nonmagmatic group IIE with those of IAB-IIICD, and with those in magmatic group IIIAB. For As, Au, W, Re, and Ir the slopes in IIE and IIIAB are similar but are less steep in IIE. For other elements IIE trends are consistent with those in IAB-IIICD, but the Ni range in IIE is much smaller than in IAB-IIICD. Differences between IIE and IAB-IIICD may reflect a lower FeS content in the IIE parental materials.

indicated by the ubiquitous presence of large troilite nodules in IAB would have been trapped.

We, therefore, support the conclusion of Wasson et al. (1980), that impacts were the source of heat and shear that produced the IAB magmas. The ubiquitous presence of silicates and the association of these with FeS nodules that can only have formed as pockets of trapped melt indicate that most IAB melts chilled rapidly and did not experience fractional crystallization. However, it seems possible that some melt pools, especially Ni-rich ones having very low cotectic temperatures, did inefficiently fractionate by crystal settling. The mechanism is probably responsible for the formation of IAB irons having Ni contents >300 mg/g.

The impact-melt model would inevitably have resulted in the occasional mixing of melts formed at different temperatures, probably when veins of high-temperature melt intersected small, low-temperature pools. This mixing offers a mechanism for forming, in close proximity, irons having similar Ni contents but different Ga, Ge, and Ir contents, i.e., irons that would be classified IIICD if concentrations of these elements were low and IAB if concentrations were high.

According to all fractionation models, the IAB irons with the lowest Ni contents offer the best estimates of the siderophile/Ni ratios in the parental chondritic materials. Normalization of IAB ratios to those in Cl chondrites shows high values (≥ 1.5) for Co, Ga, Ge, and Au. We suggest that the IAB chondritic precursors may have accreted excess amounts of a fine nebular component that carried the most volatile elements including Ga, Ge, and possibly, also Au, and that this may be responsible for part of their enhanced abundance ratios. The high Co/Ni ratio is only partly explained by this process.

Acknowledgments—We thank the many curators who have provided the meteorite samples, particularly Roy Clarke. We acknowledge with thanks several UCLA analysts who contributed to this dataset, especially Eric Jerde, Jianmin Wang, John Willis, and Lei Zhou. Alfred Kracher is thanked for a review and for insightful discussions. Henning Haack and Ernst Pernicka also provided helpful reviews. We are indebted to Pat Rogers and George Miller of the UCI reactor for a multitude of neutron irradiations. This research was mainly supported by NASA grant NAGW-3535 and its predecessor, NAG 9-40.

Editorial handling: C. Koeberl

REFERENCES

Bild R. W. (1977) Silicate inclusions in group IAB irons and a relation to the anomalous stones Winona and Mt. Morris (Wis.). *Geochim. Cosmochim. Acta* **41**, 1439–1456.

Bild R. W. and Wasson J. T. (1977) Netschaevo: a new class of chondritic meteorite. *Science* **197,** 58–62.

Buchwald V. F. (1975) *Handbook of Iron Meteorites.* Univ. California Press.

Bunch T. E., Keil K., and Olsen E. (1970) Mineralogy and petrology of silicate inclusions in iron meteorites. *Contrib. Mineral. Petrol.* **25,** 297–340.

Burnett D. S. and Wasserburg G. J. (1967) Evidence for the formation of an iron meteorite at 3.8×10^9 years. *Earth Planet. Sci. Lett.* **2,** 137–147.

Clayton R. N. (1993) Oxygen isotopes in meteorites. *Ann. Rev. Earth Planet. Sci.* **21,** 115–149.

Clayton R. N. and Mayeda T. K. (1978) Genetic relations between iron and stony meteorites. *Earth Planet. Sci. Lett.* **40,** 168–174.

Clayton R. N., Mayeda T. K., Olsen E. J., and Prinz M. (1983) Oxygen isotope relationships in iron meteorites. *Earth Planet. Sci. Lett.* **65,** 229–232.

Clayton R. N., Mayeda T. K., and Rubin A. E. (1984) Oxygen isotopic compositions of enstatite chondrites and aubrites. *Proc. 15th Lunar Planet. Sci. Conf.,* c245–c259.

Clayton R. N., Mayeda T. K., Goswami J. N., and Olsen E. J. (1991) Oxygen isotope studies of ordinary chondrites. *Geochim. Cosmochim. Acta* **55,** 2317–2337.

Dodd R. T. (1981) *Meteorites—A Petrologic-Chemical Synthesis.* Cambridge Univ. Press.

Graham A. L., Easton A. J., and Hutchison R. (1977) Forsterite chondrites; the meteorites Kakangari, Mount Morris (Wisconsin), Pontlyfni, and Winona. *Mineral. Mag.* **41,** 201–210.

Haack H. and Scott E. R. D. (1993) Chemical fractionations in group IIIAB iron meteorites: Origin by dendritic crystallization of an asteroidal core. *Geochim. Cosmochim. Acta* **57,** 3457–3472.

Herpfer M. A., Larimer J. W., and Goldstein J. I. (1994) A comparison of metallographic cooling rate methods used in meteorites. *Geochim. Cosmochim. Acta* **58,** 1353–1365.

Jones J. H. and Drake M. J. (1983) Experimental investigations of trace element fractionations in iron meteorites, II: The influence of sulfur. *Geochim. Cosmochim. Acta* **47,** 1199–1209.

Jones J. H. and Malvin D. J. (1990) A nonmetal interaction model for the segregation of trace metals during solidification of Fe-Ni-S, Fe-Ni-P, and Fe-Ni-S-P alloys. *Metal. Trans.* **21b,** 697–706.

Kallemeyn G. W. and Wasson J. T. (1985) The compositional classification of chondrites: IV. Ungrouped chondritic meteorites and clasts. *Geochim. Cosmochim. Acta* **49,** 261–270.

Kallemeyn G. W., Rubin A. E., and Wasson J. T. (1994) The compositional classification of chondrites: VI. The CR carbonaceous chondrite group. *Geochim. Cosmochim. Acta* **58,** 2873–2888.

Kelly K. R. and Larimer J. W. (1977) Chemical fractionations in meteorites-VIII. Iron meteorites and the cosmochemical history of the metal phase. *Geochim. Cosmochim. Acta* **41,** 93–111.

Kimura M., Tsuchiyama A., Fukuoka T., and Iimura Y. (1992) Antarctic primitive achondrites, Yamato-74025, -75300, and -75305: Their mineralogy, thermal history and the relevance to winonaite. *Proc. NIPR Symp. Anatarct. Meteorites* **5,** 165–190.

King E. A., Jarosewich E., and Daugherty F. W. (1981) Tierra Blanca: an unusual achondrite from West Texas. *Meteoritics* **16,** 229–237.

Kracher A. (1982) Crystallization of a S-saturated Fe, Ni-melt, and the origin of iron meteorite groups IAB and IIICD. *Geophys. Res. Lett.* **9,** 412–415.

Kracher A. (1985) The evolution of partially differentiated planetesimals: Evidence from iron meteorite groups IAB and IIICD. *Proc. 15th Lunar Planet. Sci. Conf.,* C689–C698.

Kracher A. and Wasson J. T. (1982) The role of S in the evolution of the parental cores of the iron meteorites. *Geochim. Cosmochim. Acta* **46,** 2419–2426.

Kracher A. and Willis J. (1981) Composition and origin of the unusual Oktibbeha County iron meteorite. *Meteoritics* **16,** 239–246.

Kullerud G., Yund R. A., and Moh G. H. (1969) Phase relations in the Cu-Fe-S, Cu-Ni, S, and Fe-Ni-S systems. In *Magmatic Ore Deposits* (ed. H. D. B. Wilson), pp. 323–343. Econ. Geol. Publ. Co.

Malvin D. J., Wang D., and Wasson J. T. (1984) Chemical classification of iron meteorites—X. Multielement studies of 43 irons, resolution of group IIIE from IIIAB, and evaluation of Cu as a taxonomic parameter. *Geochim. Cosmochim. Acta* **48,** 785–804.

Marti K. (1967) Trapped xenon and the classification of chondrites. *Earth Planet. Sci. Lett.* **2,** 193–196.

Mayeda T. K. and Clayton R. N. (1980) Oxygen isotopic compositions of aubrites and some unique meteorites. *Proc. 11th Lunar Planet. Sci. Conf.,* 1145–1151.

McCoy T. J., Keil K., Scott E. R. D., and Haack H. (1993) Genesis of the IIICD iron meteorites: Evidence from silicate-bearing inclusions. *Meteoritics* **28,** 552–560.

Niemeyer S. (1979a) ^{40}Ar-^{39}Ar dating of inclusions from IAB iron meteorites. *Geochim. Cosmochim. Acta* **43,** 1829–1840.

Niemeyer S. (1979b) I-Xe dating of silicate and trolite from IAB iron meteorites. *Geochim. Cosmochim. Acta* **43,** 843–860.

Olsen E. J. et al. (1994) Watson: A new link in the IIE iron chain. *Meteoritics* **29,** 200–213.

Rasmussen K. L. (1989) Cooling rates and parent bodies of iron meteorites of group IIICD, IAB, and IVB. *Phys. Scripta* **39,** 410–416.

Scott E. R. D. and Bild R. W. (1974) Structure and formation of the San Cristobal meteorite, other IB irons and group IIICD. *Geochim. Cosmochim. Acta* **38,** 1379–1391.

Takeda H. et al. (1994) Inhomogeneous distribution of materials in lodranites-acapulcoites and IAB irons and their common formation processes. *Lunar Planet. Sci.* **25,** 1375–1376 (abstr.).

Wai C. M. and Wasson J. T. (1977) Nebular condensation of moderately volatile elements and their abundances in ordinary chondrites. *Earth Planet. Sci. Lett.* **36,** 1–13.

Wai C. M. and Wasson J. T. (1979) Nebular condensation of Ga, Ge and Sb and the chemical classification of iron meteorites. *Nature* **282,** 790–793.

Wasson J. T. (1970) The chemical classification of iron meteorites—IV. Irons with Ge concentrations greater than 190 ppm and other meteorites associated with group I. *Icarus* **12,** 407–423.

Wasson J. T. (1972) Parent-body models for the formation of iron meteorites. *Proc. Intl. Geol. Cong.* **24,** 161–168.

Wasson J. T. and Kallemeyn G. W. (1988) Compositions of chondrites. *Philos. Trans. Roy. Soc. London* **A325,** 535–544.

Wasson J. T. and Ouyang X. (1990) Compositional range in the Canyon Diablo meteoroid. *Geochim. Cosmochim. Acta* **54,** 3175–3183.

Wasson J. T. and Wai C. M. (1976) Explanation for the very low Ga and Ge concentrations in some iron meteorite groups. *Nature* **261,** 114–116.

Wasson J. T. and Wang J. (1986) A nonmagmatic origin of group IIE iron meteorites. *Geochim. Cosmochim. Acta* **50,** 725–732.

Wasson J. T., Willis J., Wai C. M., and Kracher A. (1980) Origin of iron meteorite groups IAB and IIICD. *Z. Naturforsch.* **35a,** 781–795.

Wasson J. T., Ouyang X., Wang J., and Jerde E. (1989) Chemical classification of iron meteorites: XI. Multi-element studies of 38 new irons and the high abundance of ungrouped irons from Antarctica. *Geochim. Cosmochim. Acta* **53,** 735–744.

Weisberg M. K., Prinz M., Clayton R. N., and Mayeda T. K. (1993) The CR (Renazzo-type) carbonaceous chondrite group and its implications. *Geochim. Cosmochim. Acta* **57,** 1567–1586.

Willis J. (1980) The bulk composition of iron meteorite parent bodies. Ph.D. dissertation, Univ. California, Los Angeles.

Willis J. and Goldstein J. I. (1982) The effects of C, P, and S on trace element partitioning during solidification of the Fe-Ni system. *J. Geophys.* **87,** A435–A445.

Wlotzka F. and Jarosewich E. (1977) Mineralogical and chemical compositions of silicate inclusions in the El Taco, Campo del Cielo, iron meteorite. *Smithson. Contrib. Earth Sci.* **19,** 104–125.

APPENDIX

Appendix I-1. List of IAB-IIICD irons in the order of increasing Ni content

meteorite	Ni(mg/g)	meteorite	Ni(mg/g)	meteorite	Ni(mg/g)	meteorite	Ni(mg/g)	meteorite	Ni(mg/g)	meteorite	Ni(mg/g)
Itapuranga	64.5	Soledade	67.8	Hope	70.1	Bogou	73.0	Deport	80.4	Zagora	97.0
Black Mountain	64.6	Ballinger (UCL/	67.9	Rifle	70.1	Yardea	73.3	Nagy-Vazsony	80.5	Woodbine	97.0
Alexander Coun	64.7	Wichita County	67.9	Canyon Diablo	70.1	Mount Ayliff	73.4	EET 83333	80.6	Udei Station	97.1
Ballinger(AMNI	64.8	Youndegin	68.0	Smithville	70.2	Copiapo	74.0	Surprise Springs	81.3	Colfax	107.6
Magura	64.8	Gladstone (iron)	68.2	Nantan	70.3	Mundrabilla	74.7	Comanche (iron	81.9	Maltahöhe	113.6
Cosby's Creek	64.9	Lexington Coun	68.3	Mayerthorpe	70.6	ALHA77283	74.7	Southern Arizon	82.0	Anoka	118.8
Osseo	65.1	Jenny's Creek	68.3	Rosario	70.6	Ellicott	75.4	Goose Lake	82.2	Mungindi	119.3
Hasparos	65.7	Vaalbult	68.3	PCA 91003	70.8	Paracutu	75.6	Morrill	82.5	Mesa Verde Parl	120.7
Pittsburg	65.8	Morasko	68.5	Ocotillo	70.9	Waterville	76.5	Leeds	82.5	Pitts	127.0
Landes	65.8	Bolivia	68.6	Yenberrie	71.0	Thompson Broo	76.5	RKPA80226	82.9	Edmonton (KY)	129.0
Burgavli	65.9	Seymour	68.9	Dungannon	71.0	Waldron Ridge	78.0	Pine River	83.2	Lamesa	131.3
New Leipzig	66.0	Linwood	69.1	Pooposo	71.1	Wooster	78.1	Balfour Downs	83.8	Carlton	132.8
Fairfield	66.1	Jenkins	69.2	Campo del Ciel(	71.3	Masua	78.2	Karee Kloof	83.8	Egvekinot	143.0
Wolsey	66.2	Pan de Azucar	69.2	Odessa	71.9	Toluca	78.6	Shrewsbury	85.6	Dayton	170.3
Seeläsgen	66.5	Ozren	69.3	Silver Crown	72.0	Bahjoi	78.7	Zenda	87.9	Tazewell	172.1
Sarepta	66.9	Cranbourne	69.4	Neptune Mount	72.0	Annaheim	78.8	Waverley	88.6	Föllinge	177.3
Seligman	66.9	Burkett	69.5	Bohumilitz	72.2	Niagara	78.8	Harlowton	88.7	LEW 86540	182.9
Duel Hill (1873)	67.1	Coolac	69.7	Idaho	72.2	TIL 91725	79.3	Mazapil	88.7	Freda	232.9
Sardis	67.1	Oscuro Mountai	69.7	Deelfontein	72.3	Ogallala	79.7	Four Corners	90.0	San Cristobal	249.7
Jaralito	67.3	Cookeville	69.7	PGPA77006	72.6	California	79.7	Georgetown	90.1	Yamato 791694	342
Yardymly	67.4	Casey County	70.0	Bischtübe	72.7	Hatfield	79.8	Caddo County	91.7	Oktibbeha Coun	608

Appendix I-2. List of IAB-IIICD irons in the order of decreasing Ga content

meteorite	Ga(μg/g)	meteorite	Ga(μg/g)	meteorite	Ga(μg/g)	meteorite	Ga(μg/g)	meteorite	Ga(μg/g)	meteorite	Ga(μg/g)
Duel Hill (1873)	104.0	Hope	90.6	Yenberrie	83.0	Waverley	77.5	Caddo County	68.1	Mundrabilla	58.0
Morasko	103.6	Landes	89.9	Pan de Azucar	83.0	Rifle	76.8	Bischtübe	68.0	Colfax	53.6
Seeläsgen	102.9	Jaralito	89.4	PCA 91003	82.6	Waldron Ridge	76.8	Pine River	67.9	Zenda	51.4
Hasparos	101.7	Pittsburg	89.3	Nantan	82.1	Neptune Mount	76.6	RKPA80226	67.8	Four Corners	49.0
Alexander Coun	100.4	Smithville	89.0	Canyon Diablo	81.8	Comanche (iron	76.2	Ogallala	67.4	Woodbine	35.2
Soledade	98.6	Gladstone (iron)	88.9	Jenny's Creek	81.7	Odessa	75.6	Surprise Springs	66.8	Pitts	35.1
Sarepta	98.3	Burkett	88.9	Lexington Coun	81.6	Mount Ayliff	75.1	Zagora	66.3	Edmonton (KY)	24.4
Magura	98.2	Rosario	88.5	PGPA77006	81.3	EET 83333	74.8	Wooster	66.2	Maltahöhe	24.0
Sardis	97.4	Cookeville	88.1	Casey County	80.6	Paracutu	74.7	Bahjoi	66.0	Mungindi	18.8
Burgavli	97.0	Ballinger (UCL/	87.8	Pooposo	80.6	TIL 91725	73.6	Deport	64.6	Anoka	17.4
Bolivia	96.4	Yardymly	87.7	ALHA77283	80.4	Copiapo	72.3	Waterville	64.5	Lamesa	13.2
Black Mountain	96.3	Jenkins	87.6	Karee Kloof	80.4	Ocotillo	72.3	Morrill	64.0	Egvekinot	12.6
Itapuranga	94.3	Yardea	87.2	Deelfontein	80.3	Nagy-Vazsony	72.0	Mesa Verde Parl	63.1	Yamato 791694	12.2
Seligman	94.1	Seymour	86.7	Oscuro Mountai	80.2	Niagara	72.0	Shrewsbury	63.0	Carlton	11.9
Cosby's Creek	92.9	Youndegin	85.0	Annaheim	79.6	Southern Arizon	69.9	Mazapil	62.0	San Cristobal	11.1
Wolsey	92.8	Cranbourne	84.9	Ozren	79.6	Udei Station	69.3	Hatfield	61.9	Dayton	5.1
Osseo	91.1	Idaho	83.9	Bogou	79.4	Masua	69.2	Ellicott	61.5	Tazewell	4.8
Linwood	91.1	Ballinger(AMNI	83.9	Mayerthorpe	79.1	Toluca	69.0	Harlowton	59.8	LEW 86540	4.3
Campo del Ciel(	91.0	Wichita County	83.8	Dungannon	78.7	Leeds	68.9	Thompson Broo	59.7	Föllinge	3.9
Coolac	91.0	Silver Crown	83.8	Fairfield	78.4	Goose Lake	68.6	Balfour Downs	59.4	Oktibbeha Coun	3.6
New Leipzig	90.9	Vaalbult	83.7	Bohumilitz	77.6	California	68.4	Georgetown	58.3	Freda	2.1

Appendix I-3. List of IAB-IIICD irons in the order of decreasing Ir content

meteorite	Ir(μg/g)	meteorite	Ir(μg/g)	meteorite	Ir(μg/g)	meteorite	Ir(μg/g)	meteorite	Ir(μg/g)	meteorite	Ir(μg/g)
Mazapil	5.95	Copiapo	2.93	California	2.58	Surprise Springs	2.24	Rifle	1.92	Waverley	0.97
Osseo	5.85	Black Mountain	2.92	Wooster	2.58	Ballinger(AMNI	2.21	Smithville	1.90	Mundrabilla	0.91
Hasparos	5.62	EET 83333	2.88	Hatfield	2.56	Waldron Ridge	2.21	Wichita County	1.90	Hope	0.75
Wolsey	4.86	Lexington Coun	2.86	Caddo County	2.55	Neptune Mount	2.19	Rosario	1.83	Udei Station	0.68
Duel Hill (1873)	4.52	New Leipzig	2.83	Bahjoi	2.50	Mayerthorpe	2.18	Fairfield	1.79	Mungindi	0.55
Yardea	4.32	Pan de Azucar	2.81	Harlowton	2.49	Mesa Verde Parl	2.17	Colfax	1.73	Edmonton (KY)	0.50
Landes	4.26	Silver Crown	2.81	Idaho	2.49	Jenkins	2.16	Bogou	1.72	Waterville	0.35
Sarepta	4.01	Gladstone (iron)	2.79	Cookeville	2.48	Bolivia	2.15	Nantan	1.71	San Cristobal	0.33
Soledade	3.90	Linwood	2.78	Nagy-Vazsony	2.48	Youndegin	2.15	Cranbourne	1.70	Georgetown	0.25
Alexander Coun	3.73	Shrewsbury	2.77	Ogallala	2.48	Balfour Downs	2.15	Deelfontein	1.68	Yamato 791694	0.24
TIL 91725	3.67	Paracutu	2.77	Burkett	2.48	Vaalbult	2.13	Seymour	1.67	Maltahöhe	0.18
PCA 91003	3.61	Zagora	2.74	Zenda	2.47	Goose Lake	2.13	Morrill	1.60	Anoka	0.16
Magura	3.60	Coolac	2.73	Southern Arizon	2.46	Pittsburg	2.13	Yardymly	1.55	Föllinge	0.11
Annaheim	3.60	Cosby's Creek	2.72	Leeds	2.45	PGPA77006	2.11	Jaralito	1.49	Egvekinot	0.10
Yenberrie	3.50	Niagara	2.71	Four Corners	2.43	RPA80226	2.06	Casey County	1.33	Tazewell	0.09
Ellicott	3.46	Comanche (iron	2.69	Jenny's Creek	2.41	ALHA77283	2.04	Karee Kloof	1.29	Carlton	0.08
Seligman	3.30	Pooposo	2.68	Odessa	2.40	Masua	2.04	Pitts	1.22	LEW 86540	0.04
Ballinger (UCL/	3.20	Dungannon	2.66	Toluca	2.39	Bohumilitz	2.04	Burgavli	1.18	Lamesa	0.04
Campo del Ciel(	3.19	Itapuranga	2.63	Deport	2.37	Mount Ayliff	2.03	Seeläsgen	1.15	Dayton	0.03
Pine River	3.05	Ozren	2.61	Canyon Diablo	2.32	Sardis	2.01	Morasko	1.10	Oktibbeha Coun	0.03
Oscuro Mountai	2.96	Ocotillo	2.61	Bischtübe	2.31	Woodbine	1.97	Thompson Broo	1.04	Freda	0.02